DESIGN OF A SURROGATE VEHICLE TO TEST LOW SPEED PROTECTIVE DEVICES

A Thesis

by

MICHAEL W. LISK

Submitted to the Office of Graduate and Professional Studies of
Texas A&M University
in partial fulfillment of the requirements for the degree of

MASTER OF SCIENCE

Chair of Committee,	W. Lynn Beason
Co-Chair of Committee,	Joseph Bracci
Committee Member,	William Schneider
Head of Department,	Robin Auterneith

August 2015

Major Subject: Civil Engineering

ABSTRACT

Over the past few years, the public has become more aware of the number of accidents involving storefronts and pedestrians. To counteract this, protective devices are being installed to prevent errant vehicles from impacting these objects, and in order to ensure the adequacy of the protective devices, full-scale crash tests are often required. Reducing the overall cost for these tests is necessary in order to minimize the cost of these protective barriers. *ASTM F3016* recommends using a reusable surrogate vehicle to replace a full-sized pickup truck that meet the requirements of *MASH 2,270P*. The primary objective of this thesis was to design a surrogate vehicle which can be used in full-scale tests in order to meet the *ASTM F3016* standard. The secondary objective was to use non-linear finite element analysis software to validate the structural frame of the surrogate vehicle.

The surrogate vehicle design was divided into three key areas of interest. The first was the general aspects of the surrogate vehicle. The requirements of both *ASTM F3016* and *MASH 2,270P* were analyzed and incorporated when designing the surrogate vehicle. The second area of interest was the global force-deformation response of the surrogate vehicle. To ensure realistic levels of force that were exerted on the protective device, a full-scale crash test of a 2005 Dodge Ram 1500 Pickup Truck impacting a near-rigid instrumented pier was performed by Texas A&M Transportation Institute. The stiffness of the vehicle was then used to determine the force-deformation response of the surrogate vehicle. This response was obtained by

using linear compression springs. The final area of interest was the capacity of the structural frame of the surrogate vehicle. The frame was designed using a static finite element modeling software. The final frame design was then used in a non-linear finite element model to determine if any member of the frame reached the yielding stress.

Combining the general aspects, the force-deformation response, and the structural frame of the surrogate vehicle would allow for an accurate model of a full-scale crash test. This surrogate vehicle can then be used in product validation tests for new protective devices.

DEDICATION

This thesis is dedicated to my girlfriend, Samantha Grimes, my friends, and family, for their continuous love and support.

ACKNOWLEDGEMENTS

I would like to thank my committee chair, Dr. Beason, and my committee members, Dr. Bracci and Dr. Schneider, for their guidance, patience, and support throughout the course of this research.

Additionally, I would like to thank Michael Brackin and Dr. Akram Abu-Odeh for their help and support during the finite element portion of this thesis. Thanks to Michael Brackin for his assistance, guidance, and patience during the surrogate vehicle design. Thanks to Dr. Akram Abu-Odeh for his assistance and guidance in the completion of the finite element analysis portion of this thesis.

Thanks to TrafficGuard Direct, especially Mike and John Schram, for their patience, guidance, and support with the design portion of this thesis. Thanks also go to my friends and colleagues and the department faculty and staff for making my time at Texas A&M University a great and enjoyable experience. I also want to extend my gratitude to the Texas A&M Transportation Institute, which provided the means and the resources to accomplish the necessary tasks in this research.

Finally, thanks to my family for their encouragement and to my girlfriend Samantha Grimes for her patience, love, and support throughout this entire process.

TABLE OF CONTENTS

Page

LIST OF FIGURES

Page

LIST OF TABLES

Page

CHAPTER I

INTRODUCTION

Automobiles are the most common source of daily transportation in the United States. As the number of trips using automobiles increases, so does the chance of being involved with a vehicular accident. Some of these accidents involve the interaction of vehicles with buildings and pedestrians in parking lot situations. Between 1991 and 1995, buildings associated with a national convenience store chain suffered more than 1,500 vehicular collisions (Desorcie *et al.* 2013). Although the damages to the stores were a major expense to the company, driver, home owner, etc., the safety and welfare of employees and bystanders were of the upmost concern. This begs the question: are the stores and, more importantly, the pedestrians being protected from intentional or unintentional errant automobiles drivers? For many years, protective devices have been used to protect bystanders and storefronts from these types of vehicular crashes. Recently, research into protective devices, which are used in physical security applications, has become prevalent.

September 11, 2001 opened many Americans' eyes to see the vulnerability of their security systems. Therefore in 2007, ASTM International (ASTM) created a standardized test known as *ASTM F2656* (2007) to validate protective devices used in physical security (terroristic) applications. However until recently, there was no standardized testing procedure to validate any type of protective device to be used to

guard vulnerable objects from vehicular collisions. In recent months, many legislative groups, such as Miami-Dade County and the City of Artesia, have instituted new legislation requiring previously tested protective devices to be installed in front of newly constructed buildings (Miami-Dade 2012 and Artesia 2014). *ASTM F3016* (2014) was created to close the gaps in the validation process of the protective devices remaining from *ASTM F2656* (2007). This new standard focuses on errant vehicles that are traveling less than 30 mph and have a maximum gross static vehicle weight of 5,000 lbs. The requirements instituted in *ASTM F3016* (2014) were determined by attempting to reduce the overall injury of all parties involved with the accident. With this in mind, two major requirements were determined. The first requirement was identified based on the physical restraints of a parking lot where these protective devices are deployed. The second requirement was determined from the current passenger safety standards for automobiles. Current automobiles are designed with specific safety standards to protect passengers located inside the vehicle that is traveling at a speed of 30 mph.

Currently, low speed protective devices are being used worldwide to protect stores and pedestrians. These devices can be seen protecting a variety of items such as gas pumps, store entrances, store shelving, and ATMs. However, the overall effectiveness for most of these protective devices to control a vehicular collision has rarely been tested. In modern construction, protective devices are not a major component of the design and are, therefore, sometimes under designed. This leads to many of these devices being unable to control many types of vehicular collisions. Testing each and every protective device available on the market would be a very costly

adventure with the current means of testing. Therefore if protective devices are to be used after being tested, the cost to assess each device must be reduced to a more manageable amount.

The focus of this research is to use the requirements specified in *ASTM F3016* (2014) to design a reusable surrogate vehicle to be used in full-scale crash testing of protective devices. This surrogate vehicle must meet physical requirements specified in the *ASTM F3016* (2014) standard. These requirements were determined from the vehicle characteristics of a standard pickup truck set forth in the *Manual for Assessing Safety Hardware (*AASHTO *2009).* One of the benefits of using a reusable surrogate vehicle is that the overall cost of a crash test can be greatly reduced. The primary area of savings when compared to a typical crash test is that a full-scale test vehicle does not have to be purchased for each test, thus saving thousands of dollars for every test that is performed. To ensure an acceptable surrogate vehicle design is achieved, a non-linear finite element model of the surrogate vehicle will be created to validate its effectiveness. This model will be created using Hypermesh version 12.0 and then implemented into LS-DYNA to compute the finite element simulation (Altair HyperWorks 2014) (LSTC 2014).

Upon completion of this thesis, the finite element model of the surrogate vehicle can be used to assist engineers in determining whether particular protective devices would meet *ASTM F3016* (2014) standards. These finite element models can be achieved by creating a finite element model of the protective device and using the model

of the surrogate vehicle by setting it to the desired impact speed in order to determine the estimated response of the device. Design drawings for the surrogate vehicle that was modeled have been included in this thesis. Although this testing may yield conclusive results, a full-scale crash test will be necessary to determine the actual device rating.

This thesis discusses the complete process of designing and validating the surrogate vehicle that was described previously. Chapter II is the problem statement describing the overall need and the desired outcomes of this research. Following the problem statement is a detailed analysis of currently available research in this field. Chapter IV outlines the full-scale crash test of a 2005 Dodge Ram 1500 pickup truck performed by the Texas A&M Transportation Institute (TTI) to gather a baseline for the design parameters used to design the surrogate vehicle (Brackin, Menges 2014). Chapter V outlines the overall design process of the surrogate vehicle, and Chapter VI discusses the modeling and results of the finite element model created to validate the surrogate vehicle. The surrogate vehicle was compared to the full-scale crash test defined in Chapter IV to ensure the key components of the surrogate vehicle were accurately designed. The final chapter in this thesis, Chapter VII, discusses the conclusions, recommendations, and future research drawn from the results within this thesis.

CHAPTER II

PROBLEM STATEMENT

Since the invention of the automobile, society has struggled to control the number of vehicular collisions. These collisions can be separated into two distinct groups: vehicle to vehicle, or vehicle to a vulnerable object. This research is focused towards the types of collisions that are classified as vehicle to vulnerable objects. Presently, vehicle to vulnerable object collisions are still a major challenge for society to solve. Protective bollards have been developed as one method to shield vulnerable objects. ASTM International (formerly known as the American Society for Testing and Materials or "ASTM") has published a test method, *ASTM F2656* (2007), to be used in evaluating the performance of perimeter barriers including protective bollards from terroristic vehicular threats. However, the most prominent type of threat to a vulnerable object in the United States is from errant vehicles and not terroristic vehicular threats. As such, protective bollards have begun to be placed strategically around protected areas to shelter innocent bystanders from being involved in vehicular accidents.

Protective bollards have been used to guard buildings, shelving, and pedestrians for many years. These devices serve two major purposes: protect innocent bystanders and reduce the consequences associated with vehicle-into-building accidents. Desorcie *et al.* (2013) conservatively states that there is, on average, at least five vehicle-into-building accidents reported daily in the United States. Storefront Safety Council (2015)

mentions that this number could be as high as 60 accidents per day. Protective bollards are commonly installed to reduce the number of collisions involving both bystanders and buildings. Many counties are initiating new legislative items stating that protective bollards must be installed where storefront parking is available (Miami-Dade 2012 and Artesia 2014). However a large part of these devices have never been tested to see if they are adequate. The two major reasons for this are first, that there is not a current standardized test method for these devices and second, the average full-scale crash test is too expensive for the typical user to afford.

In 2007, *ASTM F2656* (2007) was developed to create a standardized test method for protective devices. This standard focuses on the terroristic threats involving all types of threat vehicles with speeds ranging from 30 mph to 60 mph. However as stated previously, the most prominent type of threat to a vulnerable object is from errant vehicles. Desorcie *et al.* (2013) states that 70% of the vulnerable objects involved in vehicular collisions are store, business, or a restaurant. These accidents occur where the overall speed of the vehicle at the point of impact is usually limited to less than 30 mph, since many parking lots are laid out in a formation that prevents higher speeds from being achieved. Therefore the ASTM F12-10 committee created a testing procedure for vehicular impacts on protective devices (including protective bollards) where the impact speeds are less than 30 mph. This new standard is called *ASTM F3016* (2014). ASTM incorporated criteria for the design of a surrogate vehicle in this standard instead of requiring a full-sized pickup truck as the threat vehicle. Using a surrogate vehicle

significantly reduces the cost of each crash test. However, *ASTM F3016* (2014) does not include an explicit definition of the surrogate vehicle to be used.

Surrogate vehicles are commonly used in the testing of vehicle safety. These vehicles allow for a greater degree of repeatability between tests with minimal to no modifications to the test vehicle. Surrogate vehicles have also been used in the testing of protective devices. In fact, some of these vehicles were designed to have a set force-deformation curve. Using surrogate vehicles also allows test agencies to reduce the overall cost of each test.

This research was directed towards designing a surrogate vehicle that can be used in conjunction with *ASTM F3016* (2014) for low speed impacts. This surrogate vehicle is to be the replacement for a 5,000 lbs pickup truck with a maximum test speed of 30 mph. It will simulate a full-scale pickup truck by modeling the force-deformation curve allowing for realistic forces to be transferred to the protective device and accurately assessing the capabilities of the protective barrier.

CHAPTER III

LITERATURE REVIEW

Over several years, many different authors have researched the design and feasibility of low speed protective devices for use in preventing damages caused by vehicular impact into vulnerable objects, particularly protective bollards. In addition, research into the design, testing, and implementation of surrogate vehicles in place of using full-sized test vehicles has been conducted. Such research has influenced committees within ASTM to incorporate surrogate vehicles into their testing methods for protective bollards. This chapter is dedicated to exploring previous research into protective bollards, surrogate vehicles, and current testing methods.

Protective Bollards

Vehicular crashes into vulnerable objects have long been a major issue across all society. Two common vulnerable objects involved in these types of collisions are storefronts and pedestrians. Storefront parking, common in modern buildings, is where vehicles pull forward into a parking spot, which is oriented towards the store. Desorcie *et al*. (2013) lists several reasons why vehicles are pulling through the parking spot and into the storefront, causing damage to the overall structure of the building and innocent bystanders. Figure III.1 shows the breakdown of the most common reasons that these accidents occur and displays that almost 73 percent of the reasons involve failure of the driver (Desorcie *et al.* 2013). When trying to find ways to prevent these accidents from occurring it is unclear how to modify the driver's behavior to reduce these types of

accidents. Therefore, it is necessary that new protective devices be developed that compensate for human error. Often times vehicular collisions involving storefronts can cost on the order of thousands of dollars. However, this cost can pale in comparison to significant injury to a pedestrian. Desorcie *et al.* (2013) states that a Nonfatal Disabling Injury costs approximately $78,700, while the death of any innocent bystander costs approximately $1,400,000. The cost per injury and the number of accidents has caused many legislative groups to take action. Locations such as Miami-Dade County (2012) and the City of Artesia (2014) are attempting to require rated protective devices to be installed wherever storefront parking is available. Although a variety of low speed protective devices are on the market, very few of them have been tested full-scale. No current protective device has been tested to the *ASTM F3016* (2014) standard rating system.

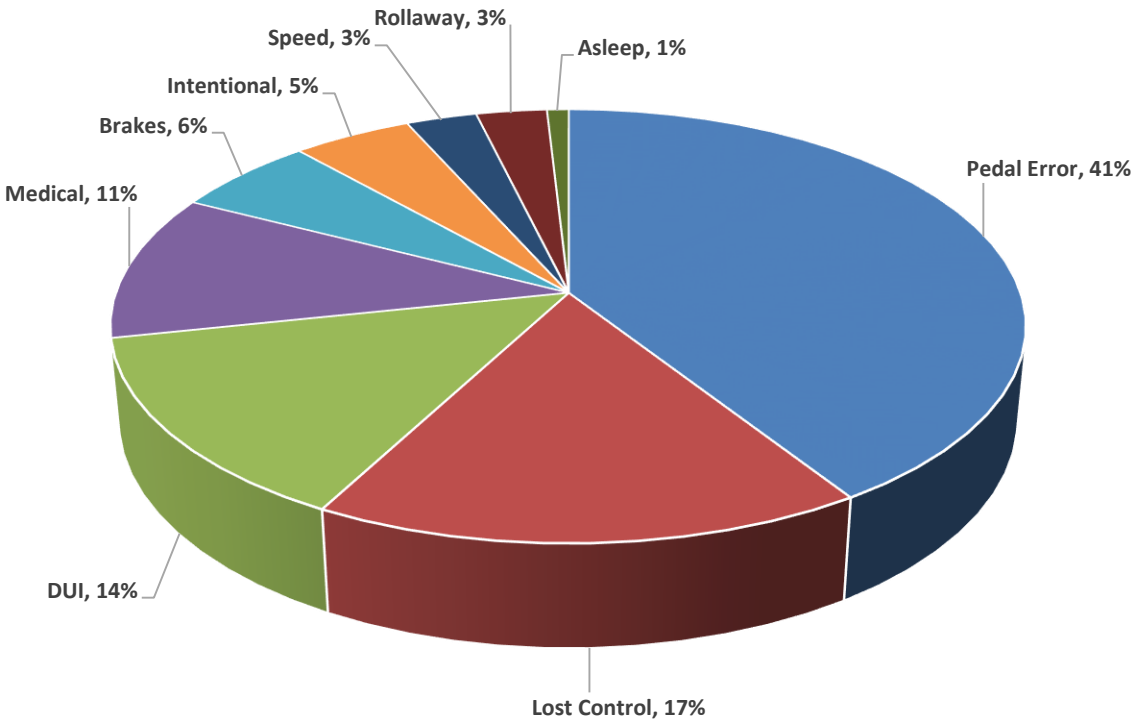

Figure III.1: Vehicle Into-Building Collisions by Cause

Since September 11, 2001, a major topic of discussion has been the prevention of vehicular terroristic threats to protected areas. The increased attention has led to the creation of a standardized test method for validating protective devices using threat vehicles ranging from small cars to large trucks. *ASTM F2656* (2007) standardizes this test method between test facilities. The primary focus of this type of testing is to protect the vulnerable objects located behind these protective devices. This standard establishes an allowable vehicular penetration when the vehicle comes to a complete stop. This allowable penetration distance provides the testing agencies with the knowledge to rate the protective device. Due to the nature of the vehicular attack (terroristic), minimum

test speeds of 30 mph must be used to comply with *ASTM F2656* (2007). Several different authors have done extensive studies on protective bollards tested according to *ASTM F2656* (2007) and the use of finite element modeling to replicate the testing scenario.

The foundation design for protective devices is a key component of the design for the system's overall effectiveness. Foundations can be classified as either small/shallow or large/deep. Engineers are always seeking new ways to accurately describe the interaction between foundations and the soil. Keske *et al.* (2014) examined the reaction of a boulder subjected to vehicular loading. A derivation of low order ordinary differential equations was created to describe the displacement for the boulder's center of mass and foundation.

Liu *et al.* (2009) focused on the interaction between shallow protective bollard foundations with the surrounding soil during a vehicle impact. A finite element analysis model was used to repeatedly change key parameters of the system in order to optimize the shallow foundation design. Using a high-fidelity-physics-based (HFPB) finite element modeling program, Liu *et al.* (2009) was able to accurately predict the effects of specific site conditions on the shallow protective bollard foundation.

A major concern for the utility companies is the longevity of their utility lines. These utility lines are shallow enough to be effected by the foundation of the protective device when it is loaded by a vehicular accident. Therefore many cities, such as New York and Washington D.C., require the end users to coordinate with all utility companies and obtain their approval before installing large foundation systems used in

protective bollard foundation (Dawson 2008). In the approval process, it is often required to verify that the utility lines will remain undamaged even when the protective bollard is loaded in a vehicular collision. Dawson *et al.* (2008) suggested using a finite element model of the proposed protective bollard system to determine the impact on the utility lines. The authors were able to predict the impact on the underground utility lines when the protective bollard is subjected to a vehicular impact. Instead of conducting a full-scale crash test, a finite element model of the protective bollard system was used to simulate a protective bollard system with all surrounding utility lines according to the *ASTM F2656* (2007) test method.

Since the *ASTM F2656* (2007) standard was created for terroristic vehicular threats, it left voids when testing common protective devices designed for vehicle to vulnerable object collisions. *ASTM F3016* (2014) was developed to fill this void and allow for the validation of non-terroristic protective devices. These non-terroristic collisions can be separated into two distinct groups: accidental and intentional. Accidental collisions occur when there is operational error that caused the vehicular crash. These collisions can be caused by pedal error, car malfunction, or medical issue. Figure III.1 shows that 41% of the time the accident is caused by pedal error (Desorcie *et al.* 2013). Intentional collisions, on the other hand, are caused by premeditated actions, such as a smash-and-grab or a robbery and account for only 5% of the total number of vehicle into-building collisions.

Surrogate Vehicles

As the demand for physical testing of protective devices increases, there has also been a need to decrease the overall expenses of a full-scale crash test. The cost of a typical crash test is approximately $50,000 (TTI 2013). To help reduce the cost of these full-scale crash tests, surrogate vehicles have been implemented in certain test situations. These vehicles can take on a variety of forms and perform many different tasks. However, every surrogate vehicle is designed to meet specific requirements, which are specific to the end goal of the test. Examples of two different types of surrogate vehicles are shown below.

- Deformable and non-deformable carts shown in Figure III.2
- Deformable and non-deformable pendulum shown in Figure III.3

Figure III.2: Deformable Surrogate Vehicle Representing a 1979 Volkswagen Rabbit.

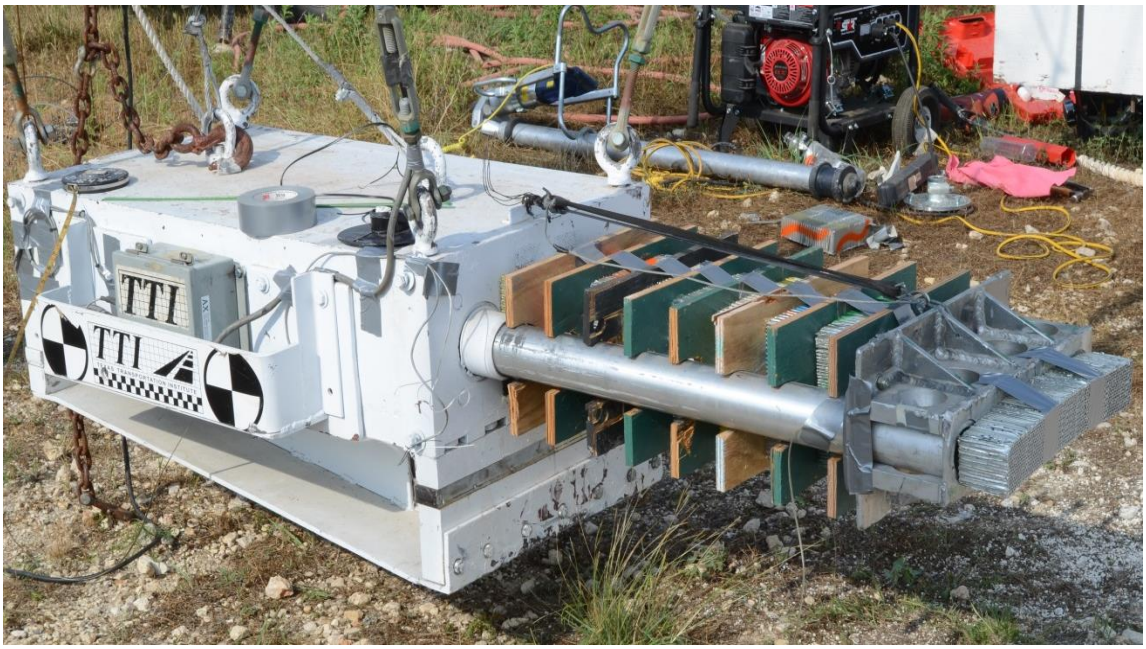

Figure III.3: Deformable 1,800 lbs Pendulum Representing a 1979 Volkswagen Rabbit.

The Federal Highway Association (FHWA) (1990) worked with the Federal Outdoor Impact Laboratory (FOIL) to create a breakaway bogie that would replicate a 1,850 lbs Volkswagen Rabbit. Figure III.2 shows a breakaway bogie. The bogie was designed to accommodate speeds up to 20 mph. One of the key design parameters was to model the slope of the force-deformation response of the 1979 Volkswagen Rabbit (Hott *et al.* 1990). The force-deformation curve relates the force imposed on the protective device due to the vehicle impact while accounting for the overall deflection of the impact vehicle. Using a rigid object as an impact device allows a force-deformation curve to be produced for these surrogate vehicles. This curve was one of the key design parameters used for the breakaway bogie. To model the force-deformation response, a honeycomb material was used with varying densities and a set area that is designed to crush at specific intervals. Table III.1 shows the different amounts of honeycomb used

to create the force displacement curve displayed in Figure III.4. Hott *et al.* (1990) tested a breakaway bogie, designed at FOIL to ensure that the surrogate vehicle meets all the design specifications. Holt *et al.* (1990) established that the FOIL breakaway bogie accurately represents realistic forces experienced by protective devices during a vehicular impact.

Table III.1: Honeycomb Configuration for Surrogate Vehicles (Hott *et al.* 1990)

Designation	**Size (in)**	**Pressure (psi)**	**Punch (in^2)**
1	2-3/4x16x3	130	-
2	Nose	-	-
3	Nose	-	-
4	4x5x2	25	-
5	8x8x3	130	21
6	8x8x3	230	15
7	8x8x3	230	6
8	8x8x3	230	-
9	8x8x3	400	21
10	8x8x3	400	12
11	8x8x3	400	-
12	8x10x3	400	-

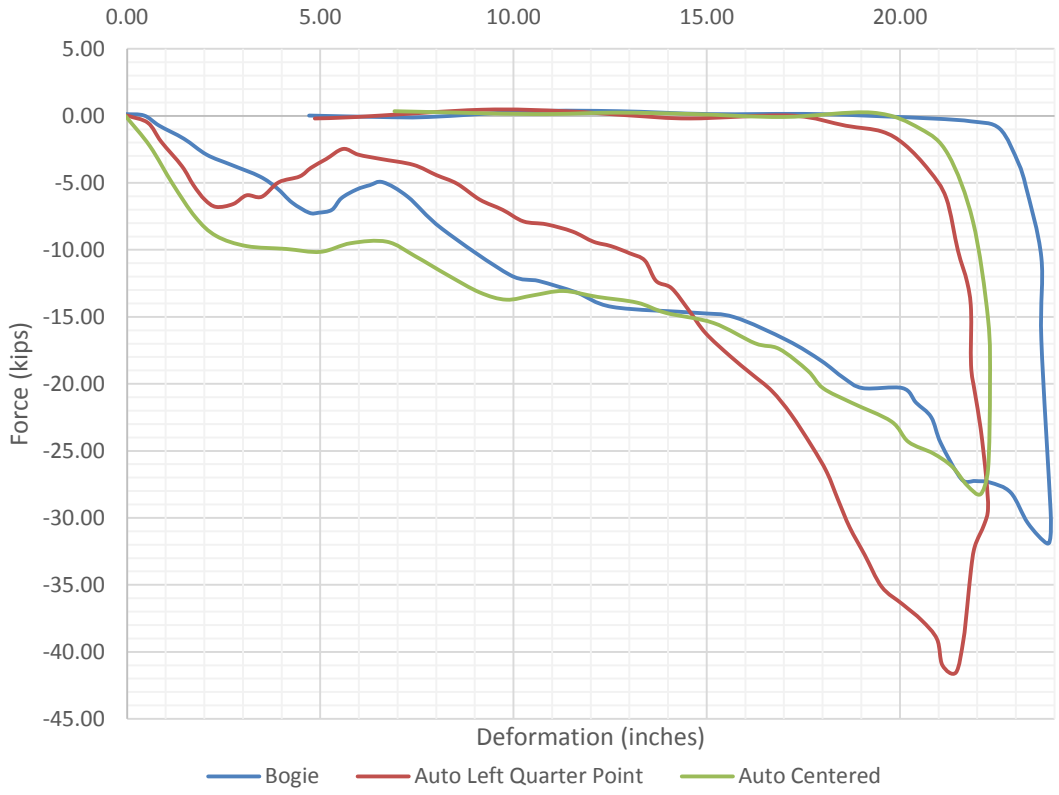

Figure III.4: Average Force Displacement Graph for the Breakaway Bogie and Volkswagen Rabbit (Hott *et al.* 1990).

Full-scale crash testing is expensive, requires multiple hours of test preparation, and does not necessarily guarantee a repeatable test. Accurate full-scale testing for minor modifications for product validation can be very expensive. Therefore FOIL validated a 1,800 lbs surrogate vehicle to be used in pendulum testing (Hott *et al.* 1990). This surrogate vehicle also uses honeycomb material to accurately depict the force-deformation response of a 1979 Volkswagen Rabbit. Table III.1 shows the configuration of honeycomb used in the 1,800 lbs pendulum and the breakaway bogie. Figure III.5 shows the force-deformation relationship between the 1979 Volkswagen Rabbit and the 1,800 lbs Pendulum. Figure III.6 shows the force vs. displacement

relationship between the breakaway bogie and the 1,800 lbs pendulum. Hott *et al.* (1990) validated the 1,800 lbs pendulum by running the surrogate vehicle through a series of tests. Holt *et al.* (1990) shows that the slope of the force-deformation response of the Volkswagen Rabbit is accurately depicted by the honeycomb configuration.

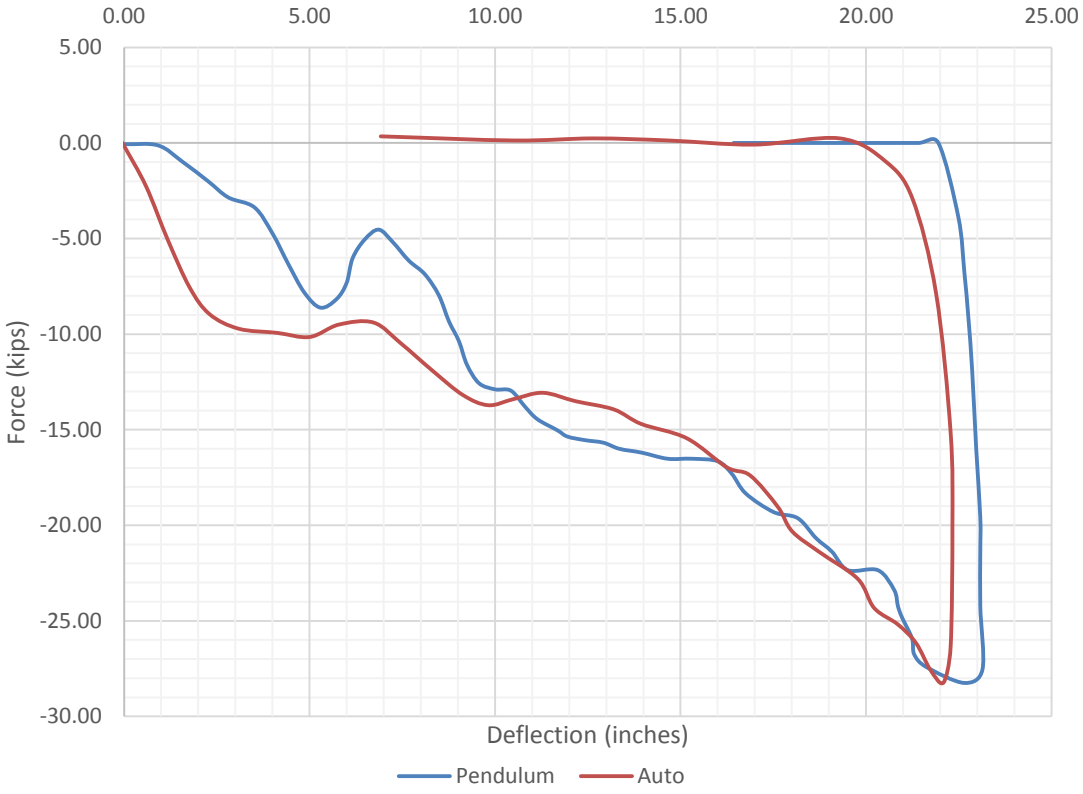

Figure III.5: Average Force Displacement Graph for the 1,800 lbs Pendulum and Volkswagen Rabbit (Hott *et al.* 1990).

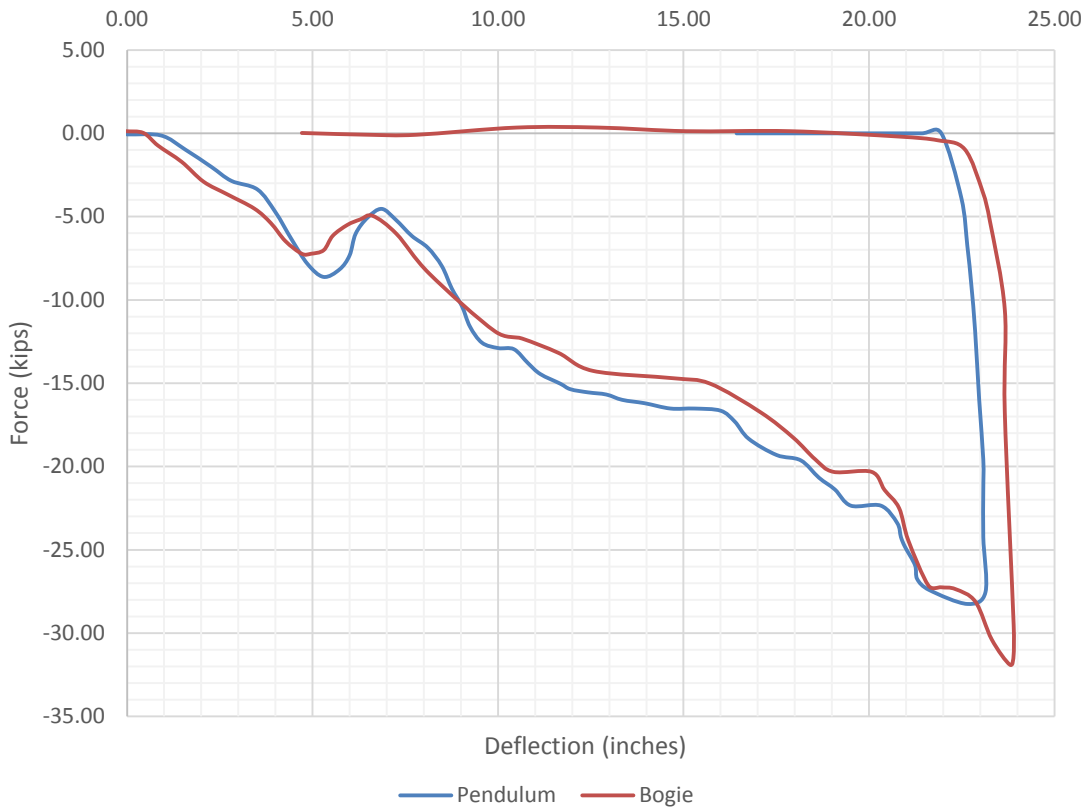

Figure III.6: Average Force Displacement Graph for the Breakaway Bogie and 1,800 lbs Pendulum (Hott *et al.* 1990).

Current Test Methods

Protective devices have become a more necessary device due to the increasing security threats posed to vulnerable objects. The United States (US) State Department requires a minimum validation test to be completed on all their protective devices (ASTM F2656 2007). To standardize regulations between test facilities, ASTM F12 committee created a standardize test method using criteria set forth by the US State Department. This test method was accepted by ASTM in 2007 and has been published as a standard titled *ASTM F2656 Standard Test Method for Vehicle Crash Testing of Perimeter Barriers* (2007). *ASTM F2656* (2007) allows test agencies to select the size of

the estimated threat vehicle, estimated threat vehicle speed at impact, and the maximum allowable penetration. The size of the test vehicle can range from a 2,430 lbs small passenger car to a 65,000 lbs heavy goods vehicle. The average threat vehicle size for a standard US State Department protective device validation test is a 15,000 lbs medium-duty truck (Hu 2011). *ASTM F2656* (2007) allows for a variety of speeds to be tested, ranging from 30 mph to 60 mph. This variability allows for the speed of the threat vehicle to be customized based upon the local conditions at the installation site. During the test, the maximum dynamic penetration is measured, which is the distance from the leading edge of the truck bed to the reference point of the protective device. The protective device is then rated by the maximum dynamic penetration of the truck. Table III.2 shows the different penetration ratings allowed by *ASTM F2656* (2007).

Table III.2: ASTM F2656 (2007) Penetration Ratings

Designation	Dynamic Penetration Rating
P1	≤1 m (3.3 ft)
P2	1.01 to 7 m (3.31 to 23.0 ft)
P3	7.01 to 30 m (23.1 to 98.4 ft)

Although the *ASTM F2656* (2007) covers the protective devices subjected to speeds between 30 and 60 mph, the average vehicular crash plaguing the general public has a typical speed less than 30 mph due to the space limitations of the parking lots. Members of the ASTM F12 committee have created a lower speed standard, *ASTM F3016* (2014), to test protective devices in which speeds are confined to a lower range (10 mph to 30 mph). This standard has many of the same principles as *ASTM F2656* (2007). The protective devices will be rated by the maximum dynamic penetration of the threat vehicle. Table III.3 shows the different penetration ratings for the proposed

low speed standard. One other primary differences between *ASTM F2656* (2007) and *ASTM F3016* (2014) is the incorporation of surrogate vehicles as a test vehicle. While *ASTM F3016* (2014) presents general design parameters for the new surrogate vehicle, an explicit surrogate vehicle design is not presented. The surrogate vehicle will replace a full sized test vehicle. This allows for increased repeatability between different crash tests and testing facilities while reducing the overall cost of the full-scale crash test.

Table III.3: ASTM F3016 (2014) Penetration Ratings

Designation	Dynamic Penetration Rating
P1	≤ 0.30 m (1 ft)
P2	0.31 to 1.22 m (1 to 4 ft)
Failure	≥1.23 m (4 ft)

CHAPTER IV

BASELINE 30 MPH PICKUP TRUCK TEST

This chapter focuses on a low speed full-scale crash test of a 2005 Dodge Ram 1500 pickup truck performed at the Texas A&M Transportation Institute (TTI) Proving Grounds. This truck impacted an instrumented semi-rigid pier at a speed of 30 mph (Brackin, Menges 2014). The crash test was performed to establish the impact conditions for this vehicle as it collides into a semi-rigid pier. This information will be incorporated in the design of a surrogate test vehicle presented in later chapters.

Impact Device Description

The impact device used for the full-scale crash test was designed and tested previously as an instrumented semi-rigid bridge pier. Minor modifications were made to adapt it to modern protective bollards.

Bridge Pier Description

The existing bridge pier consisted of a 36-inch diameter composite pipe used as a simulated semi-rigid pier supported by a braced column load frame and foundation system (Brackin, Menges 2014). The frame column was diagonally braced to a shorter vertical support anchored into the foundation. Two instrumented transducer links (load cells) were connected between the pier and the load frame. These load cells were used to measure the force of the impacting vehicle. In addition a set of accelerometers were mounted on the semi-rigid pier to account for inertia effects. The combination of load

cells and accelerometers allowed the normal force between the impacting vehicle and the bollard to be measured.

These loads cells were independently attached to the support column, and the overall height of the pier was 14-ft above the ground. Four horizontal compression arms were welded to the 1.5-inch thick vertical rib plates inside the pier (Brackin, Menges 2014). The compression arms were used to transfer the force from the pier through the instrumented load cells to the braced column load frame. The centerline elevation of the load cells coincided with the centerline elevation of the supporting pair of compression arms. The upper and lower load cells were located 12 feet and 2 feet from the top of the concrete foundation, respectively (Brackin, Menges 2014).

Modifications to the Existing Bridge Pier

An attachment was used by TTI to simulate an impact with a semi-rigid 10-inch nominal diameter bollard (Brackin, Menges 2014). The bollard attachment bolted directly to the semi-ridged bridge pier and transfers the force through it. TTI designed this attachment to fit smoothly against the bridge pier by using a curved steel plate. The plate was 1-inch thick; the inner face was curved to match the face of the existing bridge pier. The straight line distance between the inner edges at the ends of the plate was 18 inches, and the plate was 72-inches tall (Brackin, Menges 2014). Four bolt holes with a diameter of 0.875 inch were placed in the corners of the plate and were drilled so the centers of the holes are 2 inches from either edge of the plate (Brackin, Menges 2014). Three HSS10×10×0.625 hollow structural section (HSS) tubes were attached to the curved plate. One tube is placed at the center of the attachment plate, and the other

two are placed 2 inches from the top and bottom edges. Attached to the other end of the tubes was a 72-inch long 10-inch schedule 140 pipe. Inserted into the pipe was a 72 x 8.5 x 1-inch stiffener oriented in the direction of impact (Brackin, Menges 2014). The bolt pattern matched that of the attachment and positioned the bottom of the bollard 12 inches from ground level.

The complete instrumented pier with the simulated bollard attached that used by TTI is shown in Figure IV.1 (Brackin, Menges 2014). This modified pier is called the simulated bollard and is considered a semi-rigid structural object.

Figure IV.1: Simulated Bollard Prior to Testing (Brackin, Menges 2014)

Test Conditions

The test performed by TTI was completed in accordance with the specifications for *ASTM F2656* Condition Designation PU30 (2007) involving a pickup truck with a gross weight of 5,070 ± 110 lbs impacting the 10-inch nominal diameter simulated bollard at an impact speed and angle of 30 mph and 90 degrees, respectively.

Test Vehicle

A 2005 Dodge Ram 1500 pickup truck was selected to be used for this crash test. Gross static vehicle weight of the test vehicle was 5,017 lbs (Brackin, Menges 2014). The heights to the lower and upper edges of the vehicle front bumper above the ground were 13.5 inches and 26.0 inches respectfully. The height to the center of gravity of this vehicle was 28.12 inches (Brackin, Menges 2014). The test vehicle had been used in a previous crash test with minimal structural damage and is shown in Figure IV.2 (Brackin, Menges 2014).

Figure IV.2: Test Vehicle before Testing Commenced (Brackin, Menges 2014)

Test Description and Analysis

The test article was a semi-rigid 10-inch diameter by 72-inch tall instrumented, simulated bollard. The simulated bollard was selected to represent the wide array of narrow, semi-rigid bollard type perimeter security test installations. The centerline of the pickup was intended to be aligned with the centerline of the simulated bollard at the point of impact. The impact speed was intended to be 30 mph.

The 2005 Dodge Ram 1500 pickup, impacted with a speed of 30.5 mph, into the simulated bollard with the centerline of the vehicle aligned with the centerline of the

simulated bollard at an impact angle of 0.1 degrees (Brackin, Menges 2014). At 0.052 s, the front bumper began to wrap around the simulated bollard, and at 0.087 s, the pickup stopped forward motion visually (Brackin, Menges 2014). The cab of the pickup pitched downward while the tail end pitched upward at 0.103 s. Finally, at 0.106 s, the pickup began to rebound and separate from the test article (Brackin, Menges 2014).

Measured Load

A combination of load cells and accelerometers were used to capture data from both the simulated bollard and the test vehicle. To accurately describe the impact force experienced by the simulated bollard a relationship between the load cells and the accelerometers was determined. Load cells were attached between the 36-inch diameter composite bridge pier and the load frame's compression arms. Additionally, accelerometers were placed on the backside of the pier at three locations. Two accelerometers were located along the centerline of both the top and bottom instrumented pier's compression arms, while the third accelerometer was placed at height for the center of gravity of the bridge pier. The placement of these accelerometers can be seen in Figure IV.3 (Brackin, Menges 2014).

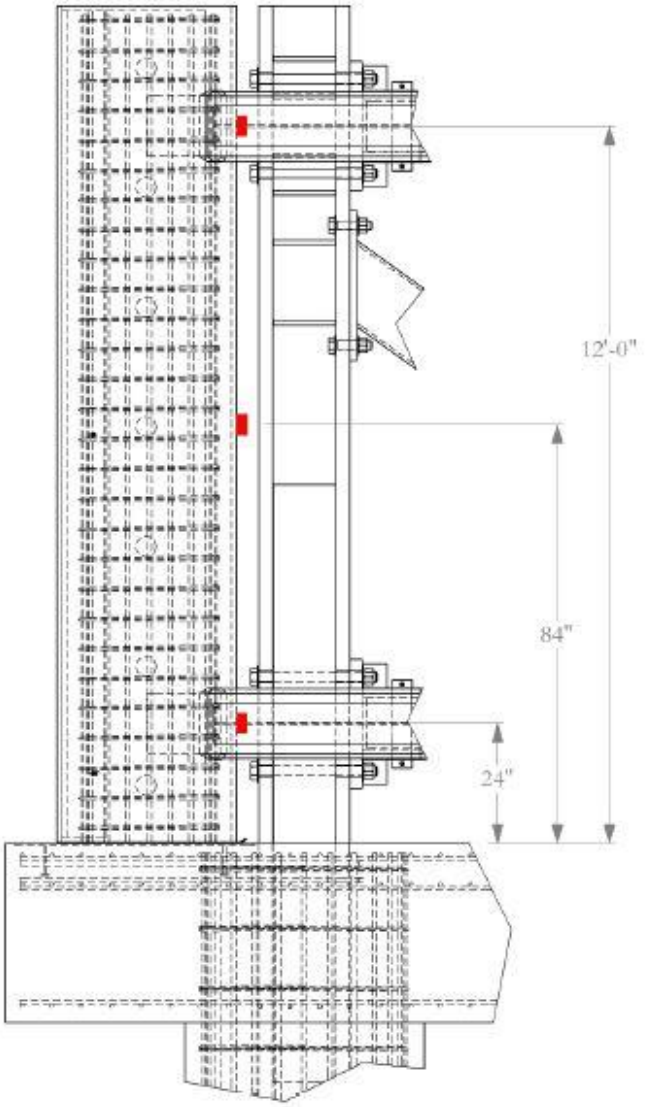

Figure IV.3: Diagram of Instrumented Bridge Pier with Locations of Accelerometers, as Depicted with Red Rectangles (Brackin, Menges 2014)

Load cells were used to measure the global force applied to the load frame of the simulated bollard. It should be noted that because of the bollard accelerations this force does not accurately describe the impact force experienced by the simulated bollard (Brackin, Menges 2014). With this in mind, Figure IV.4 shows the raw force measured

by each load cell (Brackin, Menges 2014). Using these data and engineering statics, a resultant force applied to the simulated bollard load frame can be calculated. Figure IV.5 shows this resultant force (Brackin, Menges 2014).

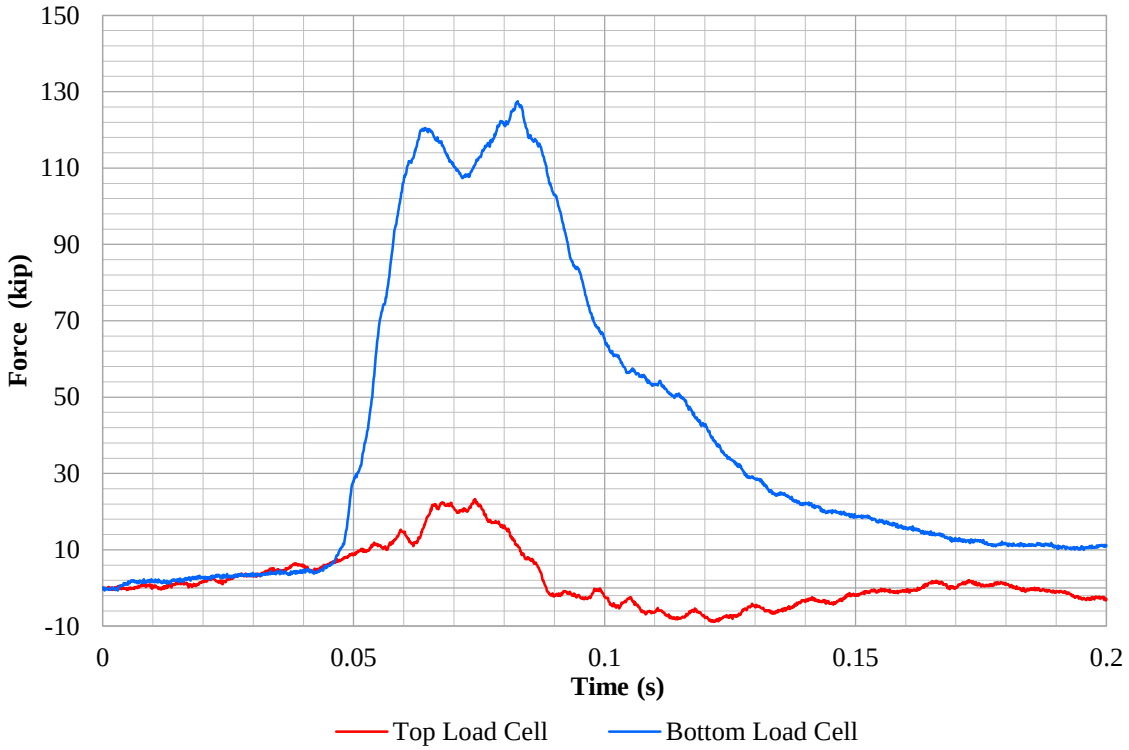

Figure IV.4: Force Measured by Top and Bottom Load Cells (Brackin, Menges 2014)

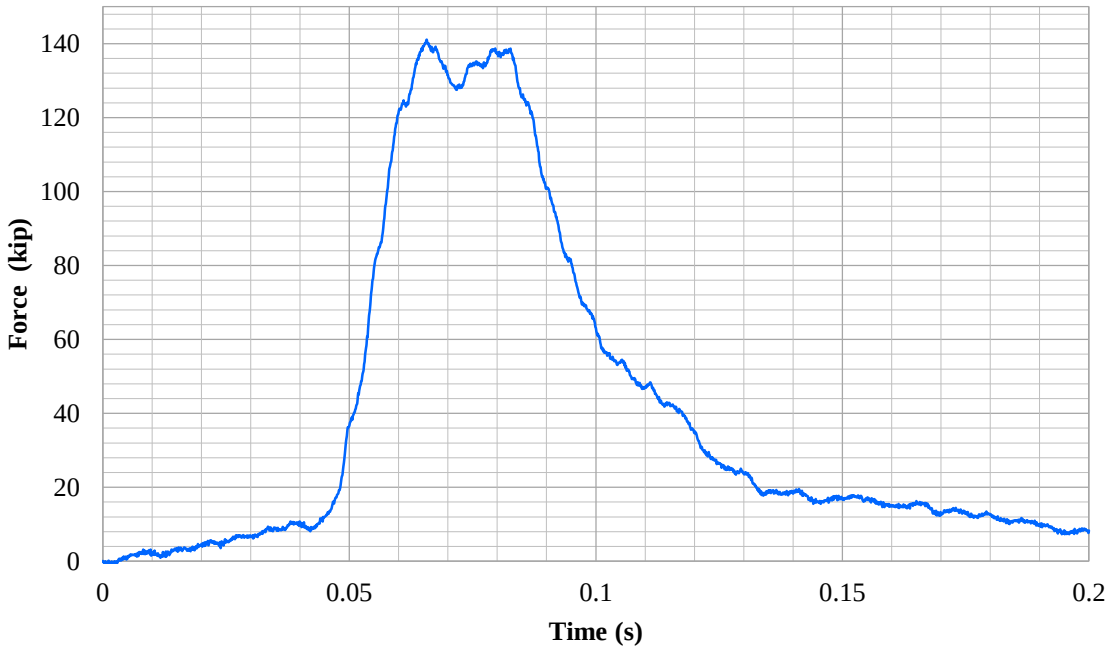

Figure IV.5: Resultant Force Measured from Load Cells (Brackin, Menges 2014)

To obtain the pickup-simulated bollard interface force, these force data presented in Figure IV.4 and Figure IV.5 must be adjusted to account for the simulated bollard's mass. This dynamic analysis is discussed below.

Researchers at TTI developed a two-degree of freedom, dynamic analysis of the simulated bollard (Brackin, Menges 2014). This analysis was performed to accurately describe the interface force and its relationship to the measured force of the load cells and the measured accelerations.

The dynamic analysis was necessary to adjust for this dynamic resistance due to the mass of the simulated bollard being approximately 700 percent larger than that of the pickup (Brackin, Menges 2014). This analysis was predicated on accurately measuring the translational and rotational accelerations of the simulated bollard. Translational

acceleration of the simulated bollard was measured using the accelerometer located at mid-height of the pier. The structural rigidity and stiffness of the simulated bollard are such that it is reasonable to take the simulated bollard as a rigid body (i.e. infinitely stiff) for use in kinematic calculations. Using kinematics, the rotational acceleration of the simulated bollard may be derived using the two accelerometers aligned with the compression arms. Data measured by these accelerometers are found in Figure A.2, Figure A.3, and Figure A.4 (Brackin, Menges 2014).

The simulated bollard's dynamic resistance is calculated by multiplying its mass by the translational acceleration measured at the center of gravity (mid-height of the pier) and in the direction of impact. Prior to calculating the simulated bollard's dynamic resistance, it is numerically necessary to filter these acceleration data using a 0.010s (10-ms) moving window average. This average was chosen over other moving averages due to amicable results from previous tests performed at TTI. These data are plotted at or near mid-time of the moving average window. This computation requires the use of a moving window average to remove extraneous high frequency data. The 10-ms time window was selected to be less than half of the period for a given natural frequency of the simulated bollard. This eliminates the possibility of removing critical dynamic response data of the structure. The natural and angular frequency of the simulated bollard was approximately 29 and 23 Hz, respectively (Brackin, Menges 2014).

Figure IV.6 shows the results of the analysis of the forces present at the interface between the pickup and simulated bollard (Brackin, Menges 2014). Further, Figure IV.6 compares these data to the original resultant force measured at the load cells (Brackin,

Menges 2014). The load cells experienced a 140 kip peak force near 0.065 s (Brackin, Menges 2014). A 120 kip peak force was measured when these data were adjusted for the simulated bollard's dynamic resistance. This value is taken to be the peak force at the interface between the pickup and simulated bollard.

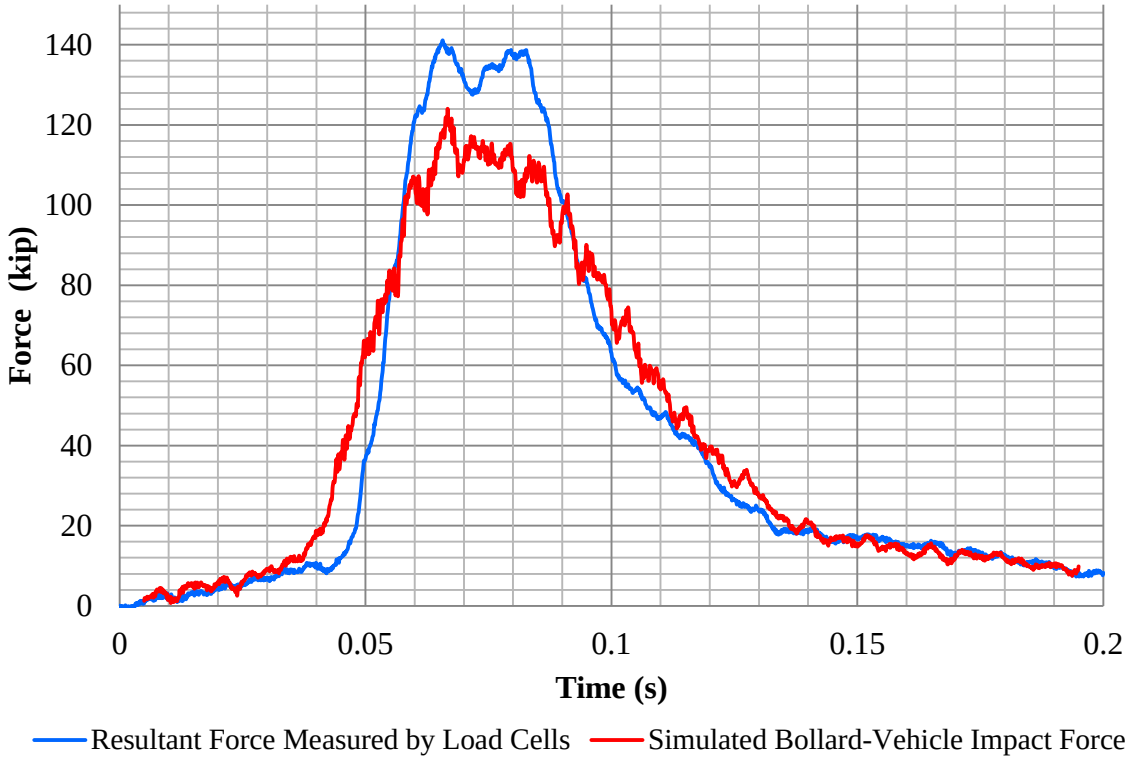

Figure IV.6: Resultant Force Measured and Simulated Bollard-Vehicle Interface Force (Brackin, Menges 2014)

Figure IV.7 shows the force at the interface between the pickup and simulated bollard. These data were averaged using 10-ms and 50-ms moving window averages. The goal of the moving averages is to filter any excessive spikes seen in the data. Through previous full-scale crash tests performed at TTI, it was shown that a 10-ms and 50-ms moving average would allow for the structure to exhibit semi-flexible and flexible

behavior, respectfully. Based on the moving averages, the estimated "peak impact force" for a 5,017 lbs vehicle impacting a narrow semi-rigid structural object (raw), semi-flexible structural object (10-ms) and flexible structural object (50-ms) at 30.5 mph are 120, 114, and 100 kips, respectively (Brackin, Menges 2014).

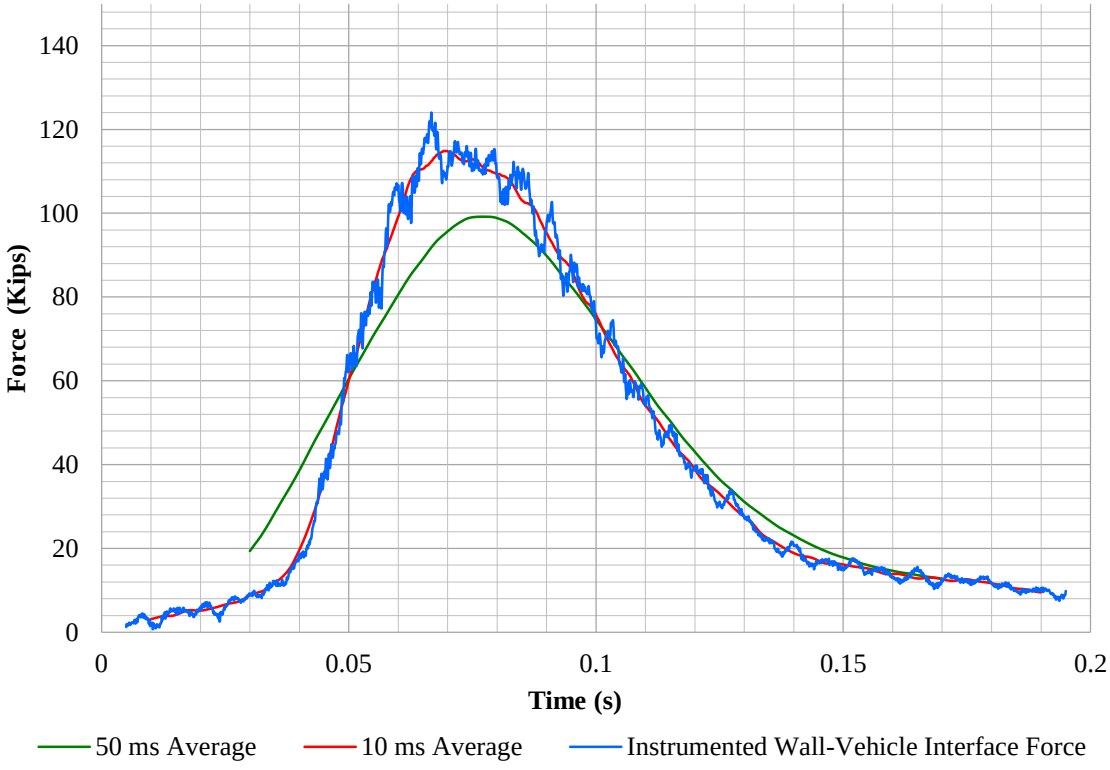

Figure IV.7: Instrumented Bollard-Vehicle Interface Force (Brackin, Menges 2014)

Further research is needed to determine the accuracy and efficiency of these moving averages aforementioned. The rationality of these estimates is based on previous experiments with amicable results performed at TTI. These moving averages provide a reasonable approach based on test data available at this time. Further, it is important to note these data do not provide a reasonable estimate of deflection or

deformation an object may experience during a vehicular impact, nor do these data indicate whether a vehicle will override an object as it deflects or deforms. To capture these phenomena in a protective device, a full-scale crash test using the protective device in question must be performed.

After further examination of Figure IV.7, it was determined that the 10-ms average removed the spikes seen in the raw data without affecting the overall dynamic response of the structure (Brackin, Menges 2014).

Linear Momentum Check

Newton's second law states that for a constant mass situation the sum of all the forces must be equal to the mass of the object times its acceleration. After integrating both sides of the equation, it can be shown that the change in the velocity times the mass of the truck over the entire time of the impact must be equal to the impulse caused by the vehicular impact on the simulated bollard. This is shown in Equation IV.1.

Equation IV.1: Integration of Newton's Second Law.

$$m_{truck} * \int_{t_o}^{t_f} a \, dt = \int_{t_o}^{t_f} F \, dt$$

In Equation IV.1 m_{truck} is the test mass of the truck, a is the acceleration of the test vehicle measured at the center of gravity of the vehicle with respect to time, and F is the impact force exerted by the truck on the structural object. Simplifying Equation IV.1, it can be seen that the change in the velocity multiplied by the mass of the vehicle must be accounted for in the impulse force response of the structure. Equation IV.2 shows us that the linear momentum of the vehicle can only be altered by changing the

mass of the vehicle and area under the force curve. For this model, it was assumed that the mass of the test vehicle does not change throughout the entirety of the full-scale test.

Equation IV.2: The change in the Linear Momentum must be accounted for in the change in the force response of the simulated bollard.

$$m_{truck} * \Delta v = \int_{t_o}^{t_f} F \, dt$$

In Equation IV.2 Δv is the change in velocity and m_{truck} is previously defined. Looking at the left hand side of Equation IV.2, there are several variables that are known. Since it is assumed that the mass of the vehicle does not change throughout the test, the first variable known is the vehicle weight which is 5,017 lbs. Using the fundamental theorem of calculus it can be shown that the integral of acceleration over the selected time interval is final velocity minus the initial velocity. Selecting t_0 to be at impact, the velocity is known to be 30.5 mph which is converted to 44.7 ft/s. Knowing that the vehicle comes to a complete stop at approximately 0.125 s, the left hand side of the equation equals approximately 6,965 lbf-s and can be seen in Equation IV.3.

Equation IV.3: Change in the Momentum from the Dodge Ram 1500 Pickup Truck Test.

$$m_{truck} * \Delta v = \frac{5{,}017}{32.2} * (44.7 - 0) = 6{,}964.59 \text{ lbf-s}$$

From Equation IV.1, the left and right hand sides of the equations must be equal. Therefore to ensure that this is true, the force curves displayed in Figure IV.10 were numerically integrated over the impact time interval. The percent error between the left and right sides of the equation were determined for the raw, 10 ms average, and 50 ms average force curves and is presented in Table IV.1. From these data, it can be seen that

the 50 ms average alters the dynamic response of the simulated bollard. Therefore the 10 ms average was used as the dynamic response of the full-scale pickup truck test.

Table IV.1: Percent Error between the Changes in the Momentum and the Area Under the Force Curve.

Force Curve	Percent Error
Raw Data	0.80 %
10 ms Average Data	0.89 %
50 ms Average Data	3.61 %

Vehicle Acceleration

Acceleration data collected from vehicles in full-scale crash tests are often used to estimate forces imposed on objects during a dynamic impact if the vehicle is not extensively deformed (i.e. loses mass). From previous tests, a 50 ms moving window average is often used with amicable results to establish an approximate impact force for design purposes. A moving average serves to filter spikes over short durations in the data. Often spikes occur as a result of noise in the data and do not accurately represent meaningful response of the structure. Alternatively, taking a time window too large will remove meaningful response data resulting in lower forces than the structure experienced.

Vehicle mounted accelerometers were used to measure the pickup's acceleration during the impact. When using vehicular acceleration, *MASH* (AASHTO 2009) recommends that accelerations be measured near the vehicle's center of gravity to capture the global response of the test vehicle. All analyses herein were performed using the pickup's longitudinal acceleration measured within the specified tolerance of the

pickup's center of gravity. Acceleration data are shown in Figure A.5, Figure A.6, and Figure A.7 (Brackin, Menges 2014).

These acceleration data measured were filtered prior to performing any calculations using these data. Typically, vehicles and their components vibrate during high speed crash tests. Vibrations introduce extraneous high frequencies or noise to the recorded data and are not meaningful to the vehicle's response. Typically, this noise is removed using filters. The correct filter must be selected to maintain the vehicle's essential structural response data without altering the dynamic response of the structure. To filter these noise data, the Society of Automotive Engineers' Instrumentation for Impact Test (*SAE J211*) provides guidelines for data reduction and filtering of data collected during vehicle impact tests (SAE J211 2007) (Brackin, Menges 2014). *SAE J211* (2007) present's information for selecting the correct channel frequency class (CFC) used to filter acceleration data for various applications. Based on the referenced material, a CFC 60 filter was appropriate for these purposes. Vehicle acceleration data used herein were filtered using a *SAE J211* class 60 filter (2007).

An approximate applied force was calculated by multiplying the pickup's longitudinal acceleration and its initial test mass. The force calculated using this method is shown in Figure IV.8 (Brackin, Menges 2014). Figure IV.8 also shows the impact force data averaged using two moving window averages, 10 ms and 50 ms (Brackin, Menges 2014). A maximum force value of approximately 295 kips was measured for the raw force, 200 kips for the 10 ms moving average, and 120 kips for the 50 ms moving average. All these values occurred near 0.08 s. From Figure IV.8, it can be seen

that the 10 ms moving average continues to follow the unfiltered data very closely (Brackin, Menges 2014). However upon closer inspection, it can be seen that the data still has large spikes in the data. Therefore, looking at the 50 ms moving average it can be seen these spikes are filtered out while the overall dynamic response of the structure is still captured. This led to the selection of the 50 ms moving average to filter the data collected from the vehicle's accelerometers.

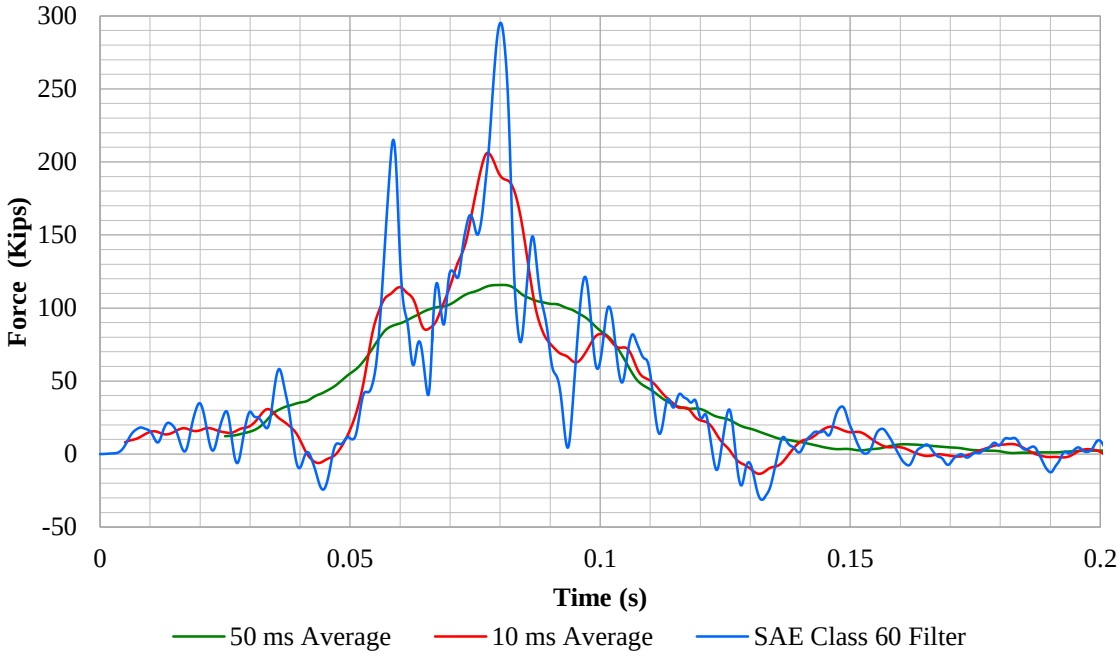

Figure IV.8: Force Calculated Using Vehicle Acceleration (Brackin, Menges 2014)

This approach requires care to calculate an applied force and is built on the assumption that the entire mass of the vehicle acts through the duration of the event. This begs the question: how accurate is the correlation between the measured forces to that which is estimated using vehicular acceleration data. Further, is the use of a 50 ms moving window average an appropriate filter to establish an approximate applied force

for design purposes? These analyses were compared, and then the 50 ms moving window average was evaluated.

Figure IV.9 compares the impact force collected from the simulated bollard to that calculated using the pickup's acceleration data without any moving averages applied (Brackin, Menges 2014). As shown in Figure IV.9, the impact force collected from the simulated bollard measured a 120 kips peak force (Brackin, Menges 2014). Using the pickup's acceleration data, the maximum force calculated was 290 kips. This 290 kips of force had a shorter duration when compared to that measured from the simulated bollard. This 290 kips force occurred near 0.08 s, while the 120 kips impact force occurred near 0.065 s and remained relatively constant through 0.08 s. Please note that these data were not averaged using the 10 ms or 50 ms moving window average.

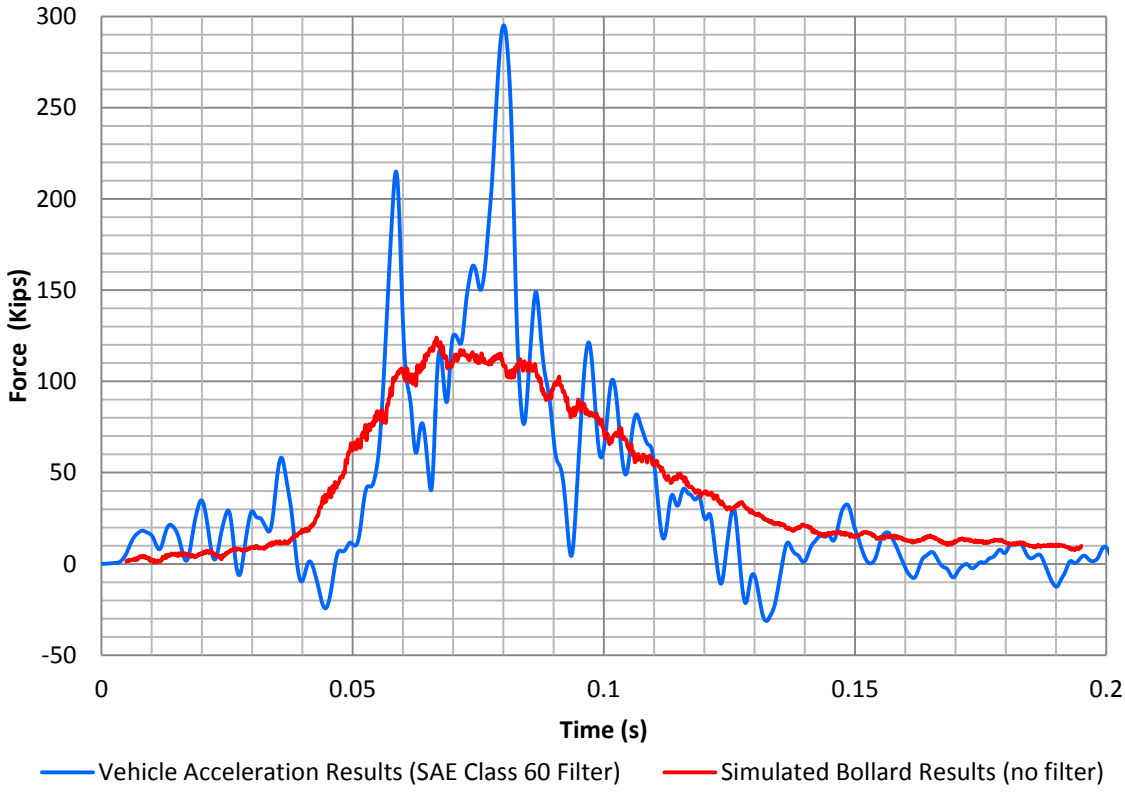

Figure IV.9: Correlation between Measured Force and Force Calculated Using Vehicle Acceleration (Brackin, Menges 2014)

To determine an appropriate structural design load, the vehicular acceleration force data shown in Figure IV.9 were averaged using a 50 ms moving window average while the impact force was filtered using a 10 ms moving average as previously explained (Brackin, Menges 2014). These averaged data are shown in Figure IV.10 (Brackin, Menges 2014). The peak applied force calculated from the vehicle's acceleration data averaged over 50 ms was 115 kips. In addition, these peak forces occur within 0.012 s from each other.

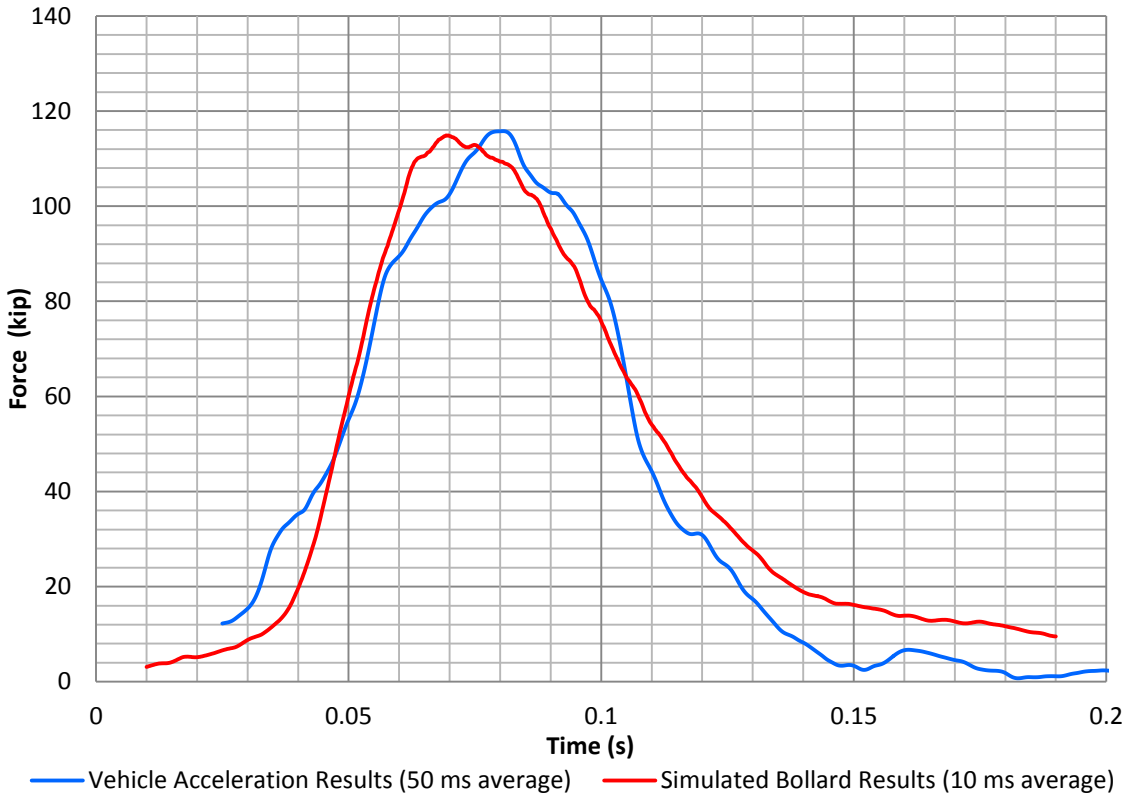

Figure IV.10: Correlation between 10 ms Moving Average of the Impact Force Measured by the Simulated Bollard to the 50 ms Moving Average of the Vehicle Acceleration Data (Brackin, Menges 2014)

From Figure IV.10 it can be seen that the data obtained from the simulated pier and the vehicle acceleration data, after applying a 10 ms and a 50 ms filter, are very similar (Brackin, Menges 2014). From this it can be assumed that the results captured from the simulated bollard accurately depict the impact force experienced by any protective device. The results of the simulated bollard were selected over the vehicle acceleration results due to the assumption that no mass was lost in the collision. In reality, a small amount of mass was lost and was not able to be accurately measured throughout the event and there was non-uniform crushing of the vehicle.

Force-Deformation Relationship

Using analytical methods, the deformation of the pickup as a function of time can be determined. The deformation was measured from the pickup's center of gravity in relation to the leading face of the simulated bollard. The maximum deformation of the vehicle measured during the test was approximately 41 inches and occurred over 0.16 s. These values are shown in Figure IV.11 (Brackin, Menges 2014).

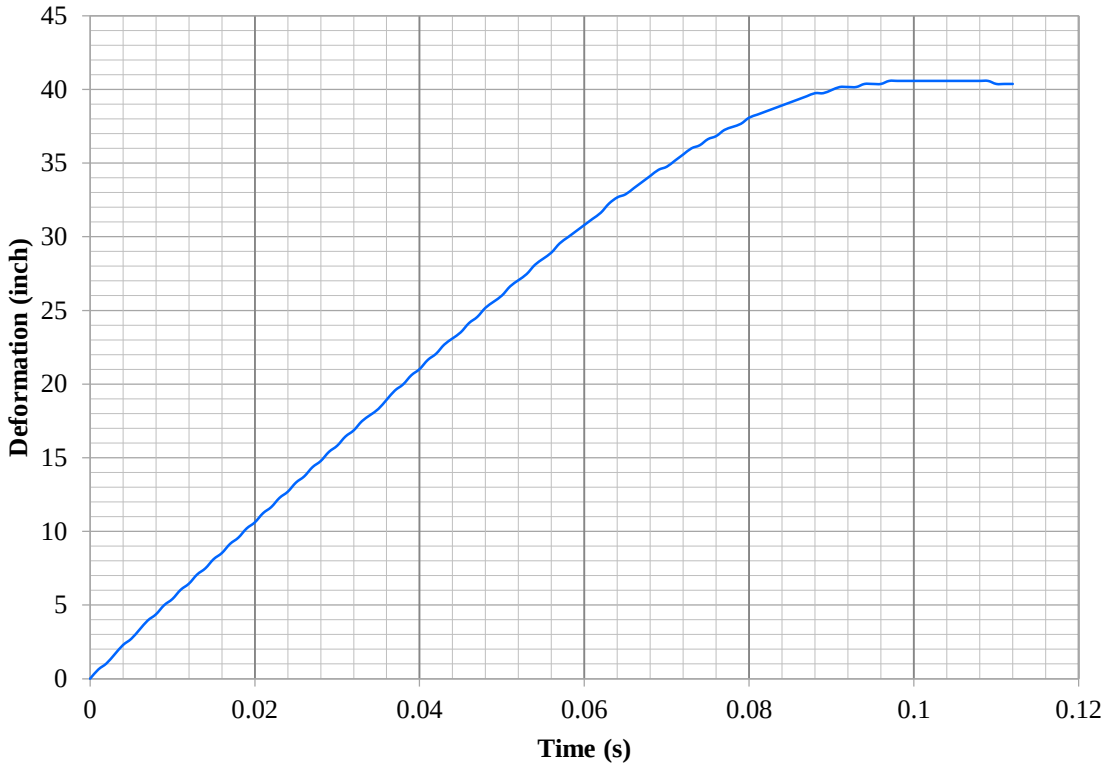

Figure IV.11: Deformation of 2005 Dodge Ram 1500 (Brackin, Menges 2014)

These deformation data may be coupled with force data measured by the simulated bollard to develop a force-deformation relationship or resistance function curve for the pickup. This force-deformation relationship for the test conditions and test vehicle described herein is shown in Figure IV.12 (Brackin, Menges 2014).

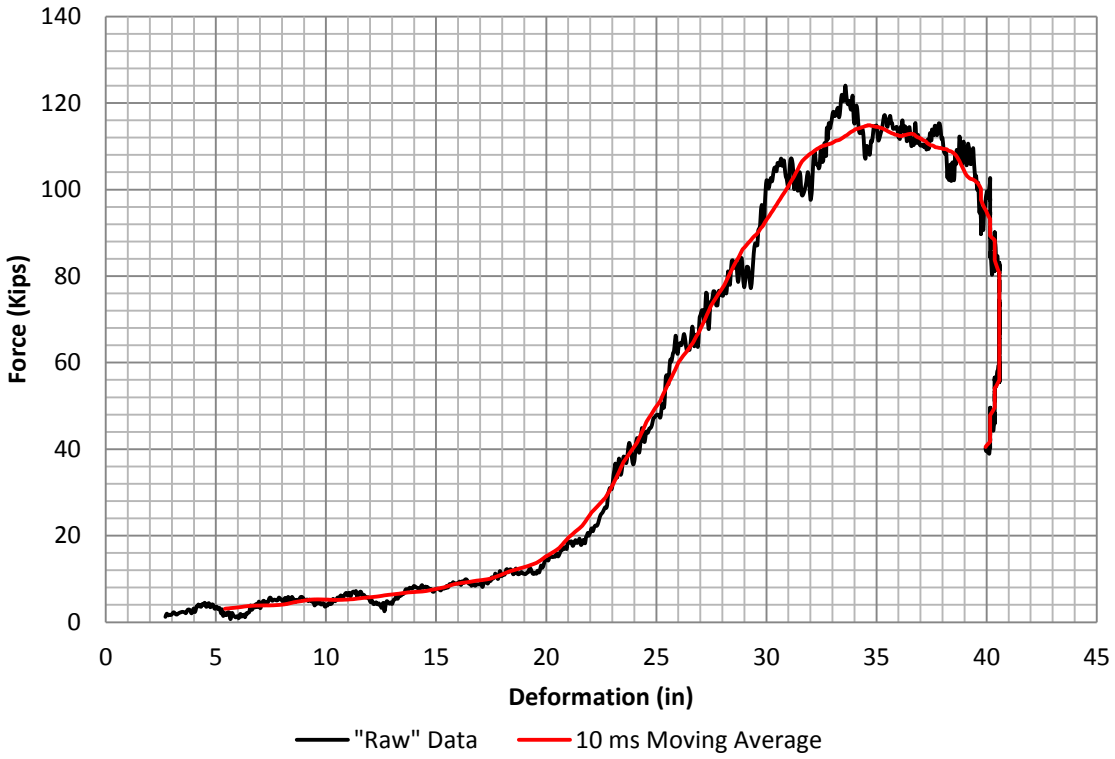

Figure IV.12: 2005 Dodge Ram 1500 Pickup Truck Force-Deformation Relationship (Brackin, Menges 2014).

From Figure IV.12, a load of approximately 12 kips was measured to have 19 inches of deformation (Brackin, Menges 2014). Beyond 19 inches of deformation, the vehicle's stiffness increased significantly to a maximum measured load of approximately 120 kips near 33.5 inches deformation. The vehicle had two discernable stages with varying stiffness. At first glance, the first stage occurred from zero to 19 inches of deformation. The second stage occurred from 19 inches through 31 inches of deformation.

Figure IV.13 shows a linear curve fit through each of these two stages (Brackin, Menges 2014). By using these curves, a linear value for the vehicle's stiffness may be

approximated for each stage. The pickup exhibited a stiffness of approximately 620 lbs/in in the first stage of the impact, while the vehicle stiffens to approximately 8,125 lbs/in during the second stage of the impact.

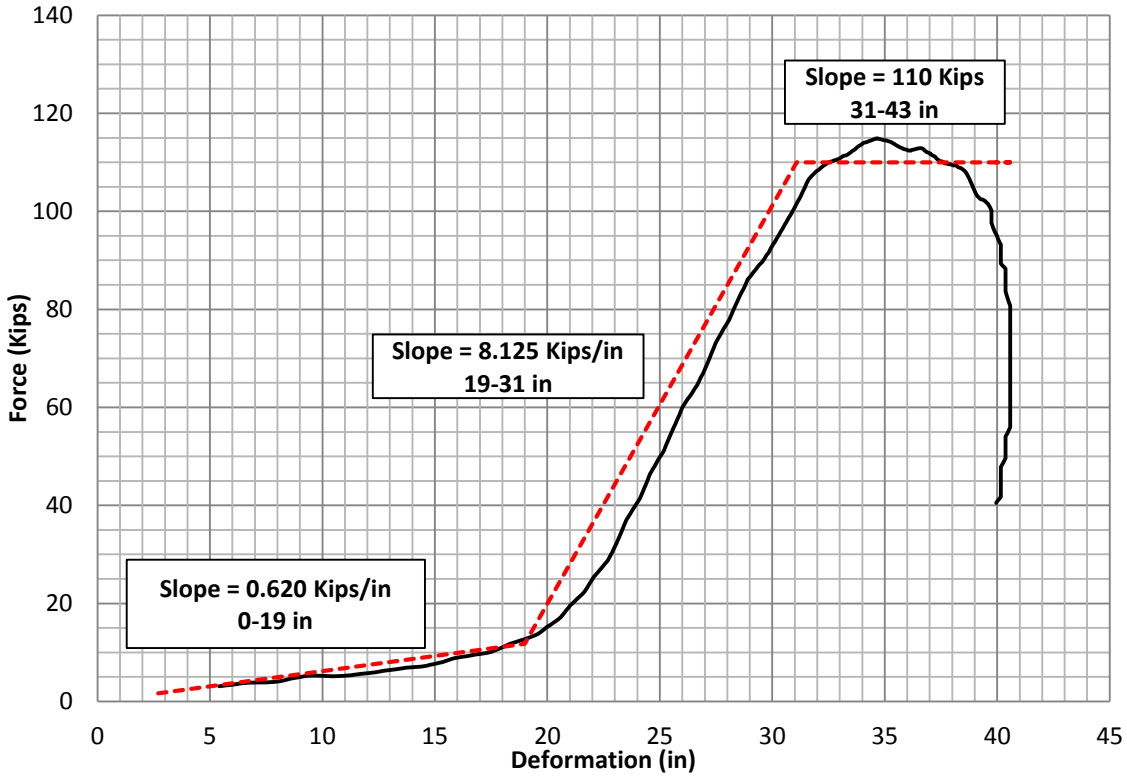

Figure IV.13: 2005 Dodge Ram 1500 Vehicle Stiffness compared to the ASTM F3016 Estimated Stiffness (Brackin, Menges 2014)

Least Squares Optimization of Linear Springs

The linear compression springs stated by *ASTM F3016* (2014) deviate from the 2005 Dodge Ram 1500 vehicle stiffness. To accurately determine the necessary stiffness in order to model the full-scale force-deformation response of this vehicle, as shown in

Figure IV.13, the principles of least squares optimization and algebra were used. The formula used for the least squares optimization can be seen in Equation IV.4.

Equation IV.4: Least squares optimization principles applied to determine the optimum spring stiffness.

$$Least\ Squares\ Optimization = \sum (F_{predicted} - F_{actual})^2$$

To obtain the predicted force, the spring stiffness and were multiplied by a small deflection of 0.25 inches. These forces were summed to obtain a predicted force deformation of the linear spring system. Three key variables were manipulated allowing for the optimization of these parameters. These three variables were the slope of the first and second segment and the intersection point. To use the least squares optimization principles, it was necessary to determine the corresponding predicted forces with the actual forces. To do this the predicted forces were linearly interpolated between surrounding points.

Using Equation IV.4, the spring stiffness and the intersection point were varied altering the sum of the least squares. This process was continued until the minimum value was obtained. When the sum of the least squares was minimized, the optimum spring stiffness and intersection point was achieved. The stiffness was varied by 50 lbs/in, and the intersection point was varied by 0.25 inches.

This research separates the force-deformation response into three distinct regions. Two of these regions use linear compression springs to achieve the desired force-deformation response. The third region is a constant force plateau used to ensure the surrogate vehicle does not exceed a maximum force exerted on a protective device. Since this force plateaus and does not attempt to model the 2005 Dodge Ram 1500

vehicle stiffness, much of this segment of the force curve was omitted from the least squares optimization principals discussed earlier. To remain consistent throughout the entire least squares optimization, the optimization was computed until the deflection reached 32 inches.

Figure IV.14 shows the results of the optimum force-deformation response predicted by the single degree of freedom dynamic analysis. Figure IV.15 compares the *ASTM F3016* (2014) predicted spring stiffness values, the optimized spring stiffness, and the 10 ms average of the full-scale crash test results. From this figure, it can be concluded that the optimized spring stiffness accurately model the 2005 Dodge Ram 1500 vehicle stiffness.

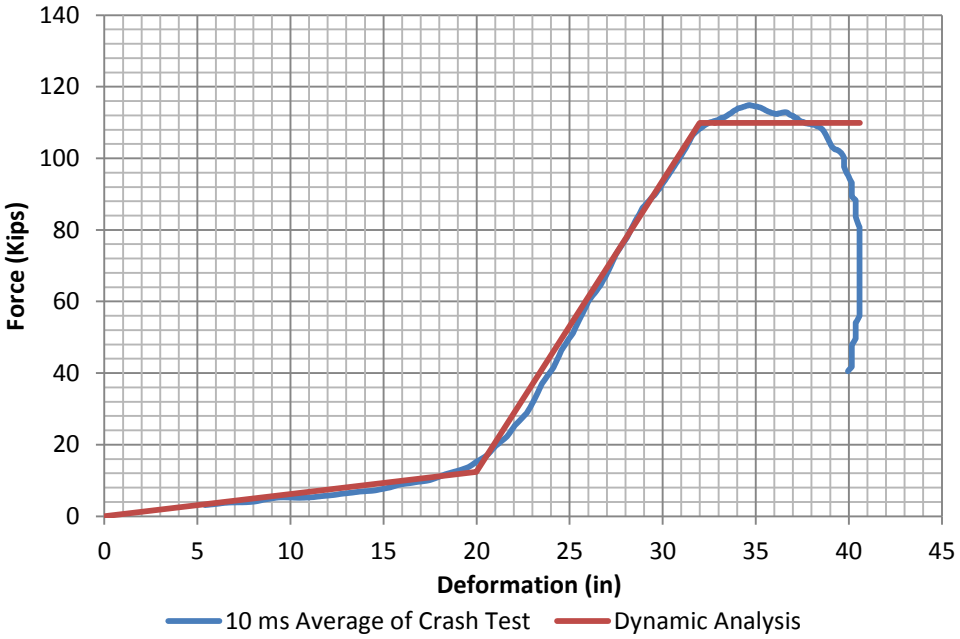

Figure IV.14: Predicted Dynamic Response of the Least Squares Optimized Linear Compression Springs.

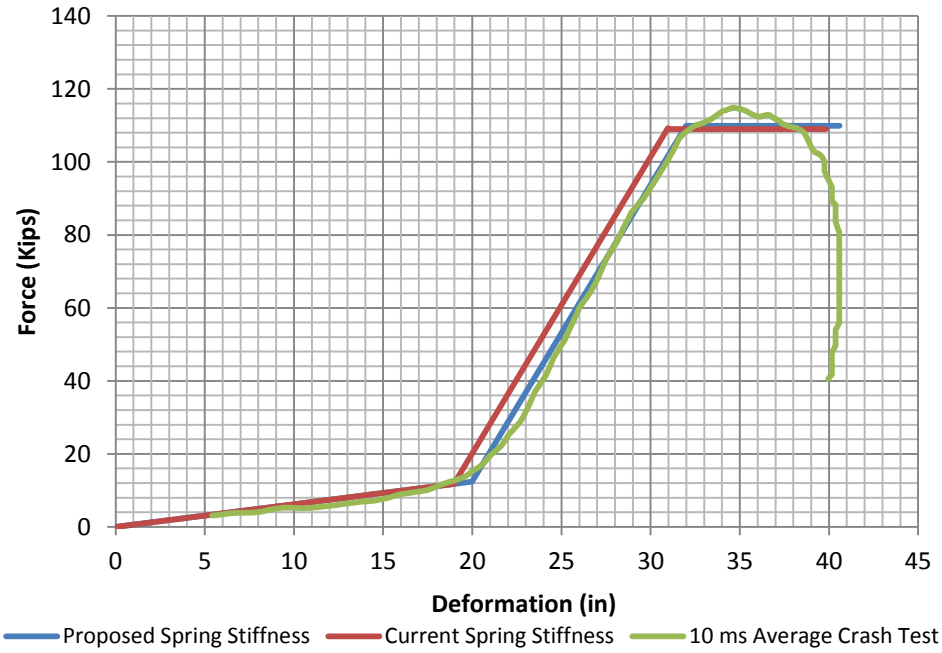

Figure IV.15: Comparison of the Current ASTM F3016 (2014) Stiffness and the Optimized Stiffness to the Full-Scale Results.

Test Vehicle Damage

Damage that occurred to the pickup truck is shown in Figure IV.16 (Brackin, Menges 2014). The cross member and steering rack were damaged, along with the front bumper, hood, grill, radiator and support, water pump and fan, motor mounts, right and left front fenders, windshield, instrument panel, floor pan, firewall, and rear of the cab. Maximum permanent deformation to the center front of the vehicle at bumper height was 28 inches.

Figure IV.16: 2005 Dodge Ram 1500 after Test is Completed (Brackin, Menges 2014)

Summary

The objective of this full-scale crash test was to determine a baseline for designing a surrogate vehicle to be used in testing of low speed protective devices. The full-scale crash test, performed by TTI, used a 5,000 lbs pickup impacting the semi-rigid bridge pier at 30 mph (Brackin, Menges 2014). Force and acceleration data were measured during this test, which complied with *ASTM F2656 PU30* (2007) and *MASH 2270P TL-1* (AASHTO 2009), into a narrow, semi-rigid structural object.

The applied force was measured using an instrumented, simulated bollard which behaved semi-rigidly during the impact. The simulated bollard was 72-inches tall and 10 inches in diameter (Brackin, Menges 2014). The simulated bollard was configured to represent the wide array of narrow bollard type perimeter security apparatuses. Vehicular accelerations were measured at the test vehicle's center of gravity (Brackin, Menges 2014). Using these data, an estimated applied force was calculated and a correlation was made between this and the measured force.

The test vehicle used was a 2005 Dodge Ram 1500 pickup that weighed 5,017 lbs (Brackin, Menges 2014). The pickup's vertical center of gravity was located at 28.12

inches (Brackin, Menges 2014). The pickup impacted the simulated bollard at 30.5 mph with its centerline aligned with the centerline of the simulated bollard. At 0.087 s, forward motion of the pickup stopped, and it began to rebound at 0.106 s.

The significant findings of the research are summarized in Figure IV.7, Figure IV.10, and Figure IV.12 (Brackin, Menges 2014). Figure IV.7 shows the applied force measured using the simulated bollard (Brackin, Menges 2014). These data shown in Figure IV.7 were averaged using a 10 ms and 50 ms moving window average to estimate the applied force to structural objects which have semi-flexible and flexible behaviors. Based on these data, reasonable peak impact forces for the design of narrow structural objects which exhibit semi-rigid, semi-flexible, and flexible behaviors are approximately 120, 114, and 100 kips, respectively (Brackin, Menges 2014).

Historically, data used to design these types of perimeter security apparatuses described herein have been based on vehicle acceleration data collected during full-scale crash tests into similar objects (Brackin, Menges 2014). These acceleration data, multiplied by the test vehicle's mass, and then averaged using a 50 ms moving window average provide an approximate force applied to the test installation. Figure IV.10 shows this force and provides a correlation to that measured using the simulated bollard (Brackin, Menges 2014). This method is based on the assumption the entire mass of the test vehicle acts through the duration of the test. For the test described, this method accurately predicted the force applied to the simulated bollard. Therefore, for an *ASTM F2656 PU30* (2007) and *MASH 2270P TL-1* (AASHTO 2009) compliant test, the use of a 50 ms moving window average to filter vehicle acceleration data and establish an

applied force provide reasonable results. Note, the pickup was not significantly deformed and little to no mass was lost during the test.

Figure IV.12 shows the force-deformation relationship for an *ASTM F2656 PU30* (2007) and *MASH 2270P* (AASHTO 2009) compliant test vehicle impacting a narrow, semi-rigid object (Brackin, Menges 2014). The maximum deformation of the pickup was approximately 41 inches. The pickup had three discernable stages of varying stiffness. Using the least squares optimization principals, these stages were identified by comparing the actual and predicted values. The first stage occurred from zero to 20 inches of deformation with a low stiffness of approximately 620 lbs/in. The second stage occurred from 20 inches through 32 inches of deformation with a higher stiffness of approximately 8,125 lbs/in. The final stage occurred from 32 inches through 44 inches with a constant force of 110 kips.

CHAPTER V

DESIGN OF SURROGATE VEHICLE

Using the full-scale crash test results from the 2005 Dodge Ram 1500 pickup truck impacting a rigid pier, discussed in Chapter IV, a surrogate vehicle was designed to test low speed protective devices. This surrogate vehicle is intended to be used as a replacement for a full-sized pickup truck traveling at 30 mph with a frontal impact into a protective device. After initial impact with the protective device, the surrogate vehicle will follow the force-deformation response determined previously that is shown in Figure IV.14.

General Characteristics

The Low Speed Surrogate Vehicle must meet several key characteristics specified by *ASTM F3016* (2014). These key characteristics can be divided into three different sections which are classified as the gross static vehicle weight, general dimensions, and the center of gravity. Table V.1 shows the requirements provided by *ASTM F3016* (2014) on the general characteristics of the surrogate vehicle.

Gross Static Vehicle Weight

The gross static vehicle weight is the overall weight of the surrogate vehicle. The requirements were selected to match the corresponding requirements for the *MASH 2,270P* (AASHTO 2009) pickup truck. The gross static weight of the surrogate vehicle should be 5,000 ± 110 lbs and should be measured when the vehicle is at rest (ASTM

F3016 2014). If additional weight is needed for the surrogate vehicle, ballast plates may be added to the structural frame to meet the necessary requirements expressed by *ASTM F3016* (2014). However this may have a significant impact on the location of the center of gravity of the vehicle. For more information on the center of gravity requirements of the surrogate vehicle, see the center of gravity subsection on the next page.

General Dimensions

ASTM F3016 (2014) provides some general dimension requirements for the surrogate vehicle. Some of these general dimensions are the wheel base, track width, the tire size, and tire inflation pressure. Table V.1 provides all the general dimensions given by *ASTM F3016* (2014) and also shows the requirements for the center of gravity, which will be explained in more detail in the next subsection.

Table V.1: General Surrogate Vehicle Characteristics provided by ASTM F3016.

Property	Specification
Wheel base	2,540 ± 125 mm (100 ± 5 in.)
Track width	1,805 mm ± 50 mm (71 ± 2 in.)
Tire size	225/75/R15
Tire Inflation Pressure (minimum)	450 kPa (65 psi)
Gross Static Weight	22,250 ± 490 N (5,000 ± 110 lbs)
Center of Gravity	710 ± 30 mm (28 ± 1 in.)

Center of Gravity

The center of gravity is a critical dimension used to determine the overall response of the surrogate vehicle. The location for the center of gravity is crucial

because the surrogate vehicle's mass will act through this point of the vehicle, dictating its global response to the protective device. It should also be noted that if the center of gravity of the surrogate vehicle is higher than the barrier, the vehicle may ride/flip over the top of the protective barrier. Therefore *ASTM F3016* (2014) sets strict requirements on the height for the center of gravity of the surrogate vehicle with respect to the ground, as shown in Table V.1. The center of gravity was set at 28 inches to match the center of gravity of a typical *MASH 2270P* (AASHTO 2009) pickup truck.

Vehicle Stiffness

Looking at Figure IV.14, it can be seen that the force-deformation response of the pickup has two distinct linear stiffness trends and one constant force region. The stiffness of these segments were previously determined to be 620 lbs/in, 8,125 lbs/in, and a constant 110 kips with respective ranges of 0 - 20 inches, 20 - 32 inches, and 32 - 44 inches. To accurately model these three stiffness ranges, a variety of devices were considered. The plausible devices range from hydraulic dampeners to linear compression springs to constant honeycomb segments. The linear compression springs were determined to be the most cost efficient and effective device. To ensure that the stiffness increases at the correct deformation, two different springs with varying stiffness were used. The first spring has a stiffness of 620 lbs/in and extends far enough to deflect a total of 32 inches. The second spring has stiffness of 7,505 lbs/in and only extends far enough so that it will begin adding additional stiffness after the first 20 inches of deformation. The 7,505 lbs/in spring should be long enough to allow for a minimum of 12 inches of deformation. These linear compression springs were aligned with the center

of gravity of the surrogate vehicle to reduce any adverse effects and to prevent them from locking. A series of HSS pipes were primarily used to prevent these springs from buckling. As a secondary use, these HSS pipes were used as a spring stop, preventing the springs from crushing more than the desired length. For the constant 110 kips section, a honeycomb material was determined to be an effective material to achieve the plateau in the force diagram. There are currently a variety of densities for the honeycomb material currently on the market. For this application a 399 psi honeycomb material was utilized to obtain the desired force. Knowing the crushable force of the material, the size of the honeycomb material could be calculated from the force required by *ASTM F3016* (2014). It was determined that the necessary area of 399 psi honeycomb material was 13.5 x 21.34 inches. For the ease of fabrication the area was rounded to 13.5 x 21.0 inches providing a crushable force of 109 kips. The combination of the linear compression springs and the honeycomb material will now be referred to as the linear compression spring system. This linear compression spring system should be aligned with the center of gravity of the surrogate vehicle. This will prevent any form of loading other than pure compression due to any eccentricity of the springs or rotation of the surrogate vehicle from occurring.

Single Degree of Freedom Dynamic Analysis

A single degree of freedom dynamic model was developed to model the linear compression spring system of the surrogate vehicle (Biggs 1964). It has been previously proven that an effective model of a car crash can be created using linear springs (Emori 1968). Figure V.1 shows the single degree of freedom dynamic model created to

analyze the linear compression spring system. This model uses a mass cart to resemble the surrogate vehicle moving at a speed of 30 mph towards a rigid object. There are three springs that will resemble the linear compression spring system for the surrogate vehicle. Spring 1 has a stiffness of 620 lbs/in and crushes for a total length of 32 inches. Spring 2 has a stiffness of 7,505 lbs/in, which crushes for a total length of 12 inches and only engages after the first 20 inches of deformation. Subsequently, springs 1 and 2 combine together to provide a total spring stiffness of 8,125 lbs/in. Spring 3 is a constant force spring which is used to resemble the honeycomb material. In this application, the honeycomb will compress at a force of 109 kips. The basis for the single degree of freedom dynamic analysis of the linear compression spring system is that as the time increases the mass cart moves closer to the rigid object. Knowing the spring stiffness and the distance the cart moves forward, the spring force resisting the forward motion can be determined by using Hooke's Law.

When performing this single degree of freedom dynamic analysis, the time step of the model needs to be carefully selected. Too large of a time step will not accurately show the true dynamic reaction of the linear compression springs and can lead to numerical instability of the model. Too small of a time step increases the total number of data points used for this model but will also increase the accuracy of the model. The proper selection of a time step will be discussed later.

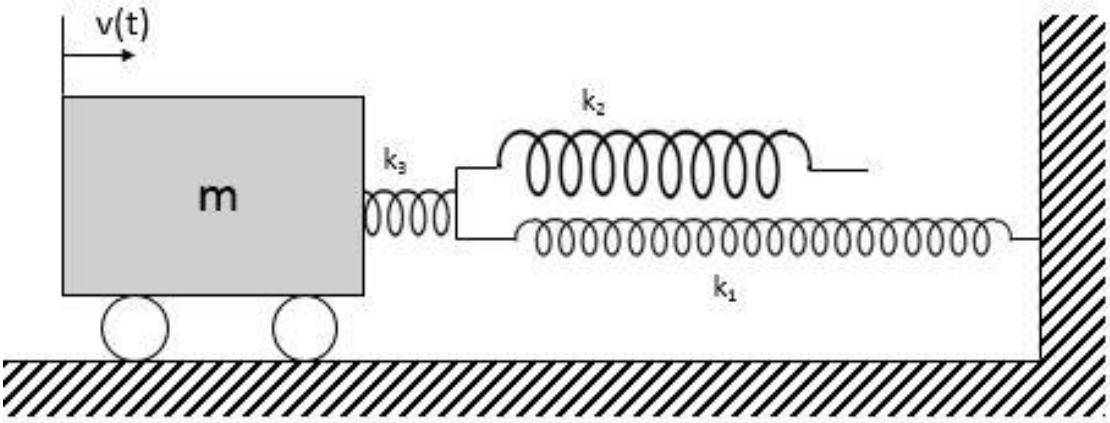

Figure V.1: Illustration of Single Degree of Freedom Dynamic Model used to Test the Linear Compression Spring System.

Selection of a time step that is small enough to accurately capture the behavior of the dynamic behavior of the object is critical to the accuracy of the model. To ensure that a proper time step has been selected a variety of time steps were used as a computation time step in the single degree of freedom dynamic model. Figure V.2 shows the force vs time comparison of these models with different time steps. Figure V.3 shows a detailed view of the transition between the linear compression springs and the honeycomb material. It can be seen that as the time step decreases the deviation between these points becomes minute. Therefore using these figures, a time step of 10^{-4} was selected. This time step was deemed better than 10^{-5} because the time intervals aligned with full-scale crash data compiled from the Baseline Pickup Truck Test better.

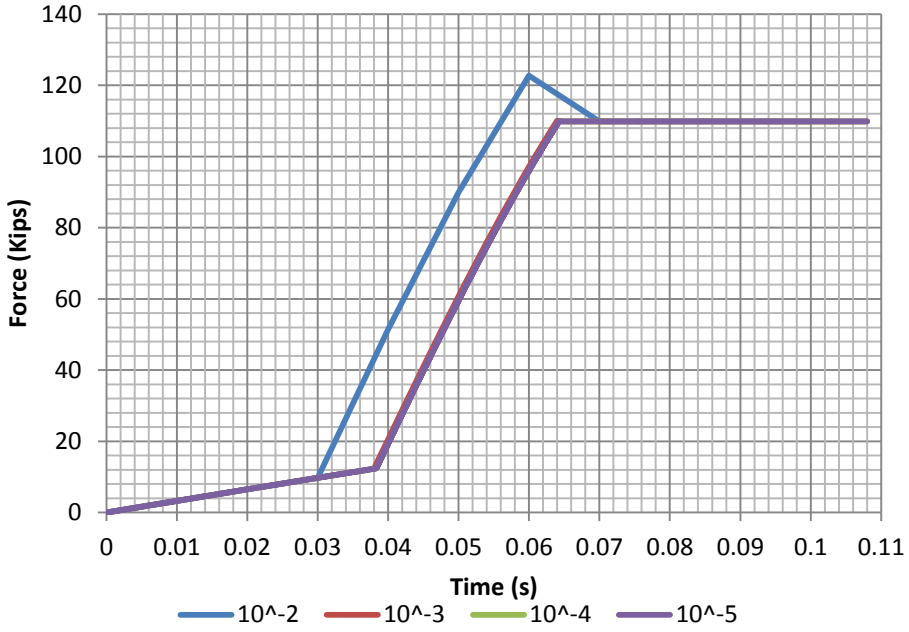

Figure V.2: The Single Degree of Freedom Dynamic Response with Different Time Step Intervals.

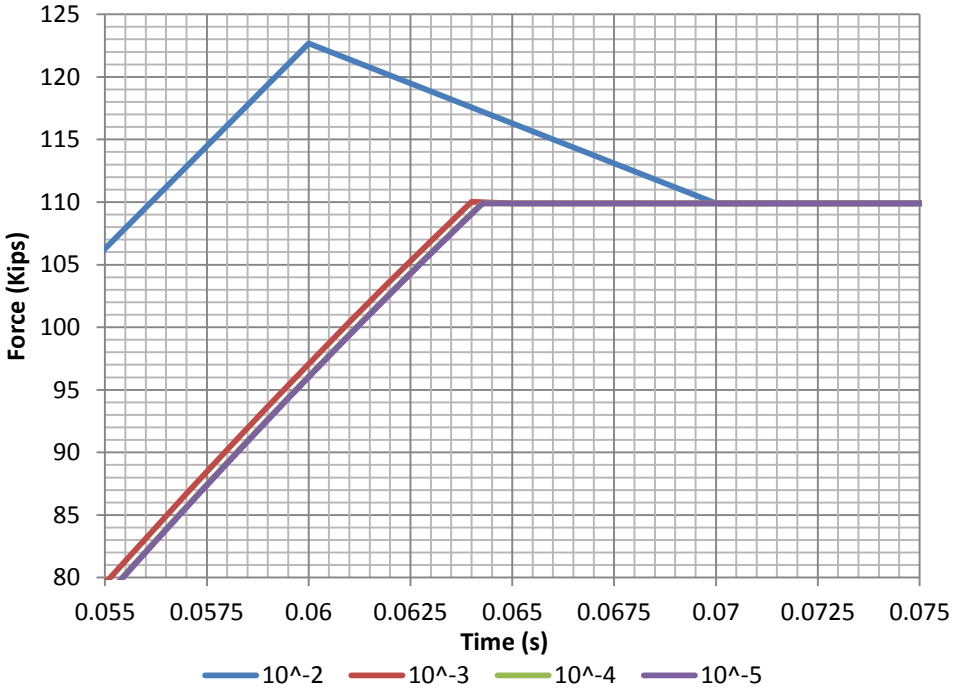

Figure V.3: Critical Area of the Graph where the Linear Compression Springs End and the Honeycomb Material begins to Crush.

Using this dynamic analysis model shown in Figure V.1, a force vs time graph of the model can be generated and compared to the Baseline Pickup Truck test found in Chapter IV. Figure V.4 shows the comparison of these two curves. Using the same model, a deformation vs time and a force vs deformation response can be generated. Figure V.5 and Figure V.6 show the comparison of the deformation vs time and the force vs deformation between the single degree of freedom dynamic model and the Baseline Pickup Truck test.

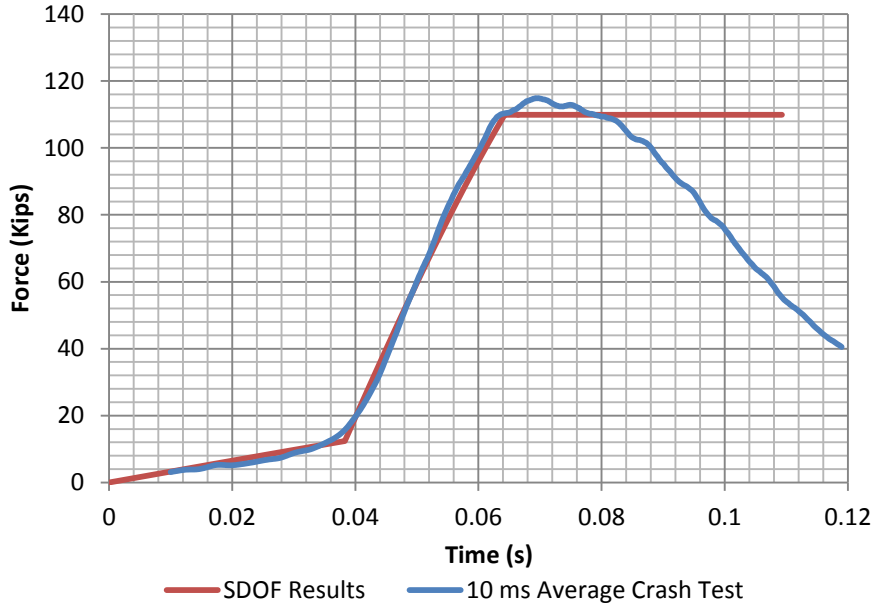

Figure V.4: Force vs. Time Comparison between the Single Degree of Freedom Dynamic Analysis and the 2005 Dodge Ram 1500 Pickup Truck.

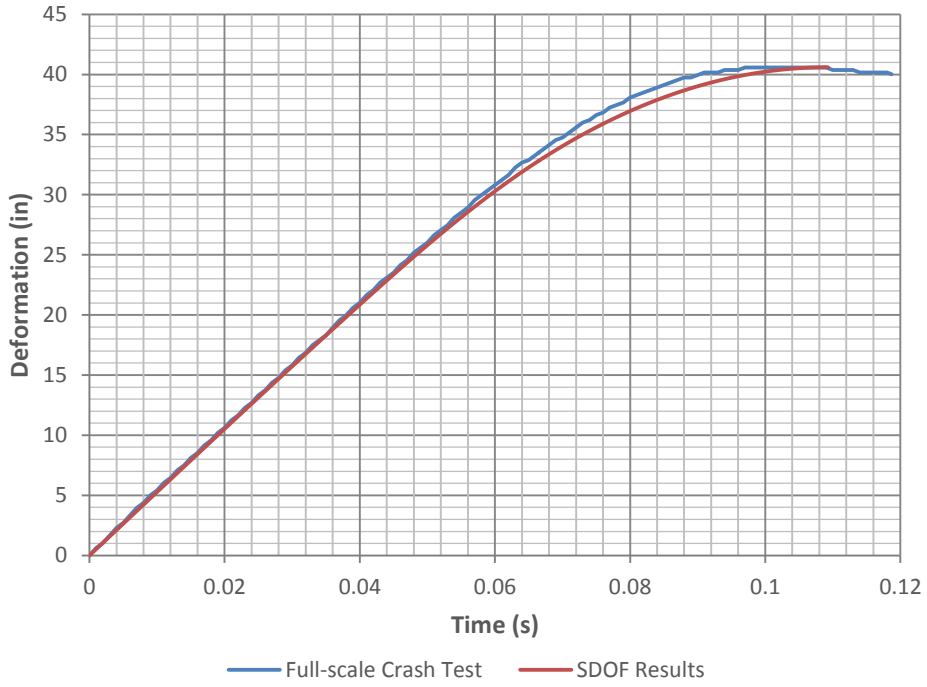

Figure V.5: Deformation vs. Time Comparison between the Single Degree of Freedom Dynamic Analysis and 2005 Dodge Ram 1500 Pickup Truck.

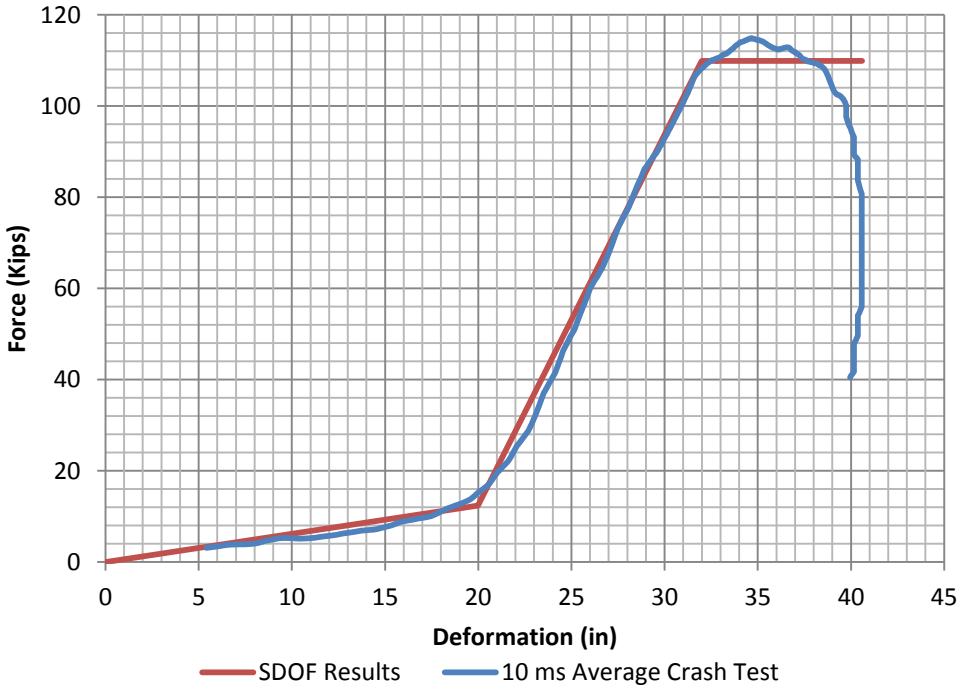

Figure V.6: Force vs. Deformation Comparison between the Single Degree of Freedom Dynamic Analysis and the 2005 Dodge Ram 1500 Pickup Truck.

Figure V.4 shows that the single degree of freedom dynamic analysis model of the linear compression spring system produces a force vs time curve that is very similar to that measured during the full-scale crash test of the 2005 Dodge Ram 1500. Using this graph, the constant force located in the third segment of the force curve was determined to remain constant for 12 inches. The crushable length of 12 inches was determined to ensure the total area under the force curve for the Baseline Pickup Truck test was completely accounted for in the modeled force curve of the surrogate vehicle, but it allows for more crushable length than necessary. This was done to ensure that the load applied to the frame is not any higher than the 115 kips it was designed to withstand by preventing the springs from bottoming out which would cause a large increase in the force exerted on the bogie.

Figure V.5 shows the deformation vs time curve for the single degree of freedom dynamic analysis model compared to that of the Baseline Pickup Truck test. At the maximum deformation, the dynamic analysis model of the linear compression springs had a 2.56% difference from the deformation curve captured from the Baseline Pickup Truck test. This is associated to the slight difference between the stiffness of the springs and the stiffness of the test vehicle. Another distinction between the two tests is the impact velocity. The 2005 Dodge Ram 1500 pickup truck had an impact velocity of 30.5 mph while the single degree of freedom dynamic analysis model of the linear compression springs assumes an impact velocity of 30 mph.

Figure V.6 shows the difference between the force vs deformation curves of the dynamic analysis model of the linear compression springs and the Baseline Pickup Truck test. There is a slight difference between these two curves with the majority of the difference focused towards the second and third stages of the stiffness of the surrogate vehicle. As explained earlier, the differences in the curves were caused by the difference between the stiffness captured in the Baseline Pickup Truck test and the modeled stiffness of the surrogate vehicle. Another difference can be associated to the impacting velocities between the test vehicle and the surrogate vehicle.

.

Vehicle Frame

To contain the force caused by the compression of the linear springs, a structural frame is required. As the surrogate vehicle is traveling toward the protective device, the springs will compress, causing the vehicle to come to a halt. When the springs are fully compressed, the estimated force can be approximately 115 kips. To prevent any permanent damage to this structural frame, a dynamic load factor of 2.0 was applied to the total load of the structural frame. Therefore a structural frame was designed to resist a total force of 230 kips. This structural frame was designed with HSS 3.5 x 3.5 x 0.25 Grade 50 tubing. The frame was designed to remain below the yield limit of the material's stress-strain response, therefore preventing any permanent deformation.

Static Analysis of Structural Frame

The structural frame was analyzed using Sap 2000. A model of the structural frame was created in Sap 2000 and can be seen in Figure V.7. From the surrogate

vehicle design drawings, located in Appendix B, it can be seen that the linear compression spring system is connected to a ½" steel plate. This steel plate rests against the back members of the structural frame. Therefore in the Sap 2000 model, a distributed load was placed along the edges of the structural members where the steel plate would be pushing against the structural frame. These loads were appropriately distributed by drawing the possible yield lines of the plate and taking the load associated with the areas formed by these yield lines. Taking the total load, a distributed load can be calculated for all four contact areas. Another key component of the model is the boundary conditions. For the structural frame model, the boundary conditions were assumed to be pinned at the rear four corners of the frame as seen in Figure V.7. This assumption is conservative because as the surrogate vehicle is moving forward, the weight will act through the center of gravity. Since it is not practical to hold the center of gravity constant, the rear portion of the frame was assumed that the weight of the vehicle would act through the structural frame.

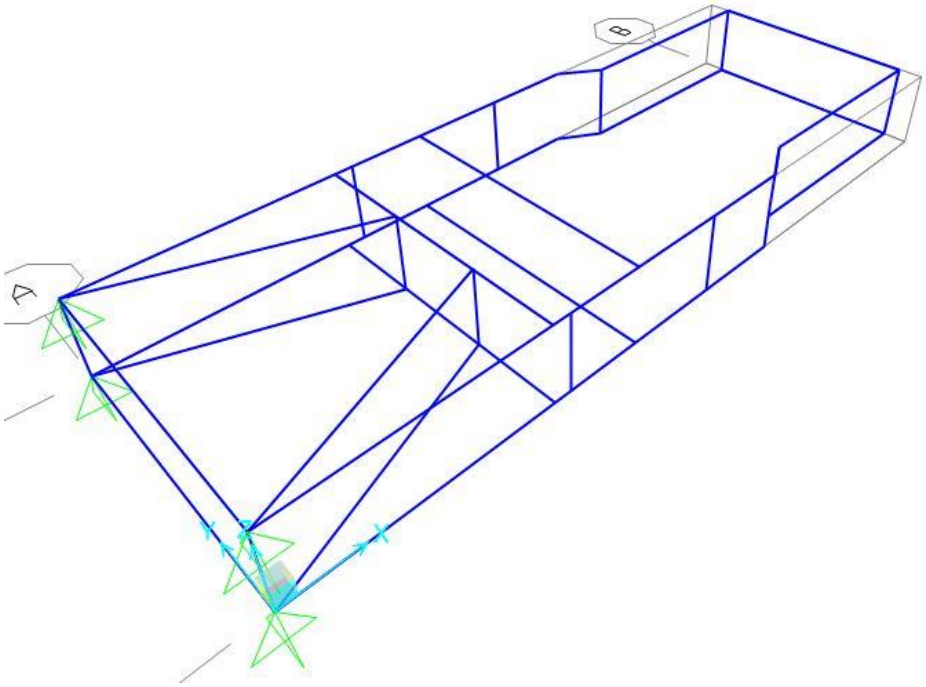

Figure V.7: Image of Sap 2000 Model of the Structural Frame for the Surrogate Vehicle.

To convert the dynamic load to a static load, a dynamic load factor was applied to the maximum measured force in the full-scale crash test. This is a common practice in structural engineering. Many different studies have been completed to determine the appropriate dynamic load factor necessary for the loading type of the study. For a compression spring, the maximum dynamic load factor was determined to be 2.0 (Wright 2012). The structural frame was analyzed for axial, shear, horizontal moments, and vertical moments. These forces are shown on the Sap 2000 model of the structural frame in Figure V.8, Figure V.9, Figure V.10, and Figure V.11, respectively.

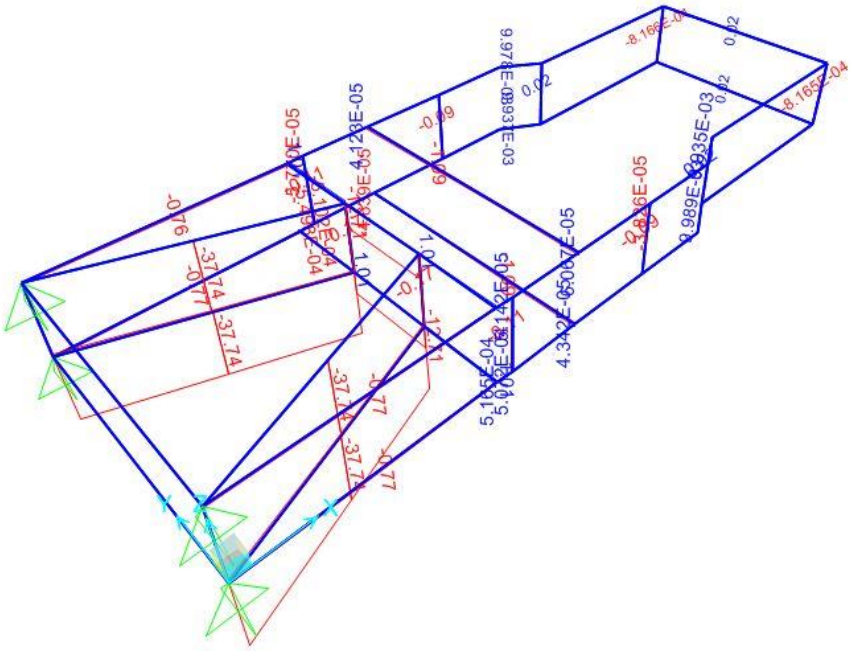

Figure V.8: Axial Forces Outputted from the Sap 2000 Model.

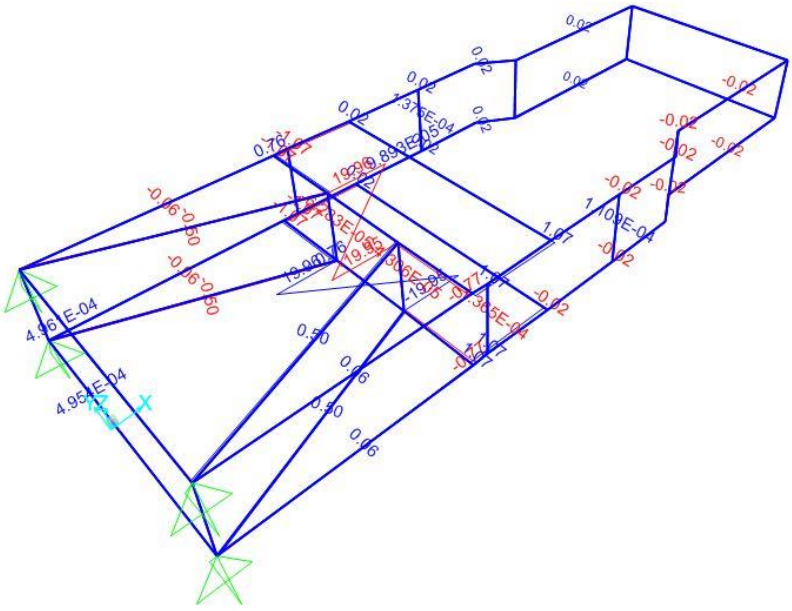

Figure V.9: Shear Forces Outputted from the Sap 2000 Model.

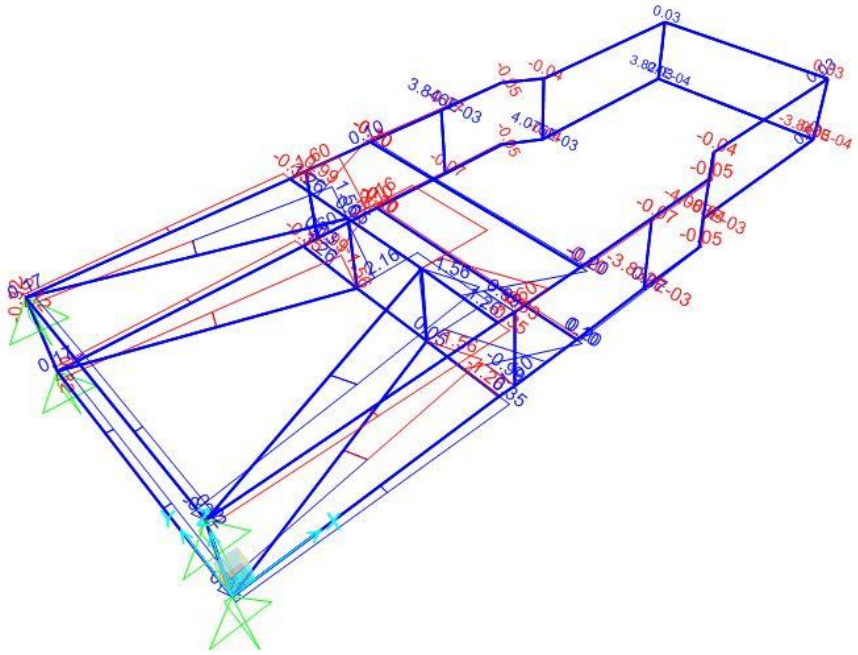

Figure V.10: Horizontal Moments Outputted from the Sap 2000 Model.

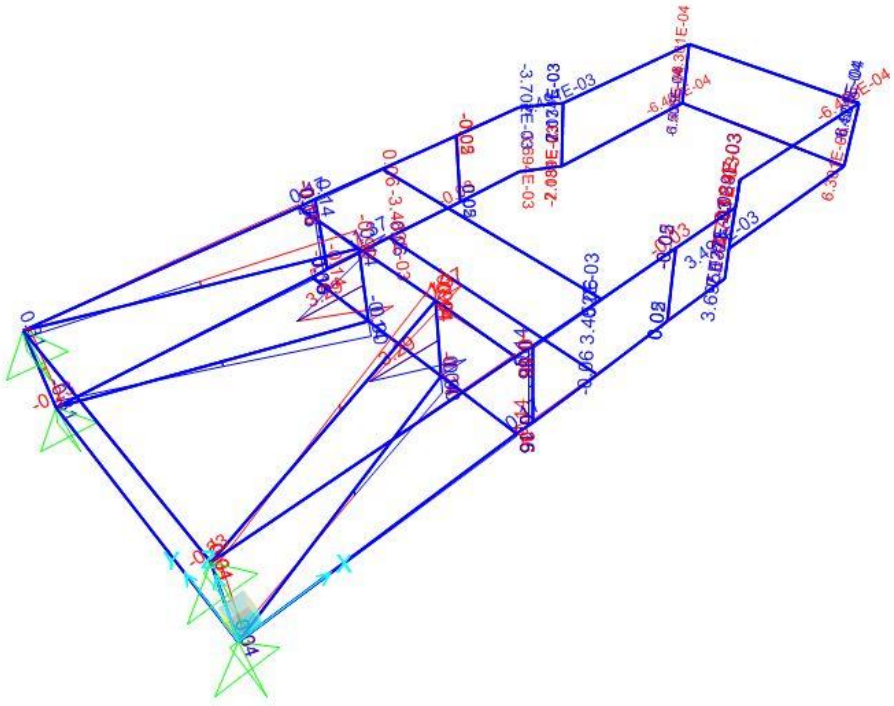

Figure V.11: Vertical Moments Outputted from the Sap 2000 Model.

The forces depicted above were then combined using the beam-column equations found in the AISC Steel Manual 14th edition (2012). This equation is dependent on the total axial load divided by the critical axial load in order to determine the ratios for combining all the stresses from the axial, horizontal, and vertical moments. These equations take a fraction of the force divided by the critical counterpart force and add them together. Summing the ratios of forces across each region of the member must be less than 1.00 to be deemed acceptable. Figure V.12 shows the structural frame with color coding associating to the sum of all the critical ratios.

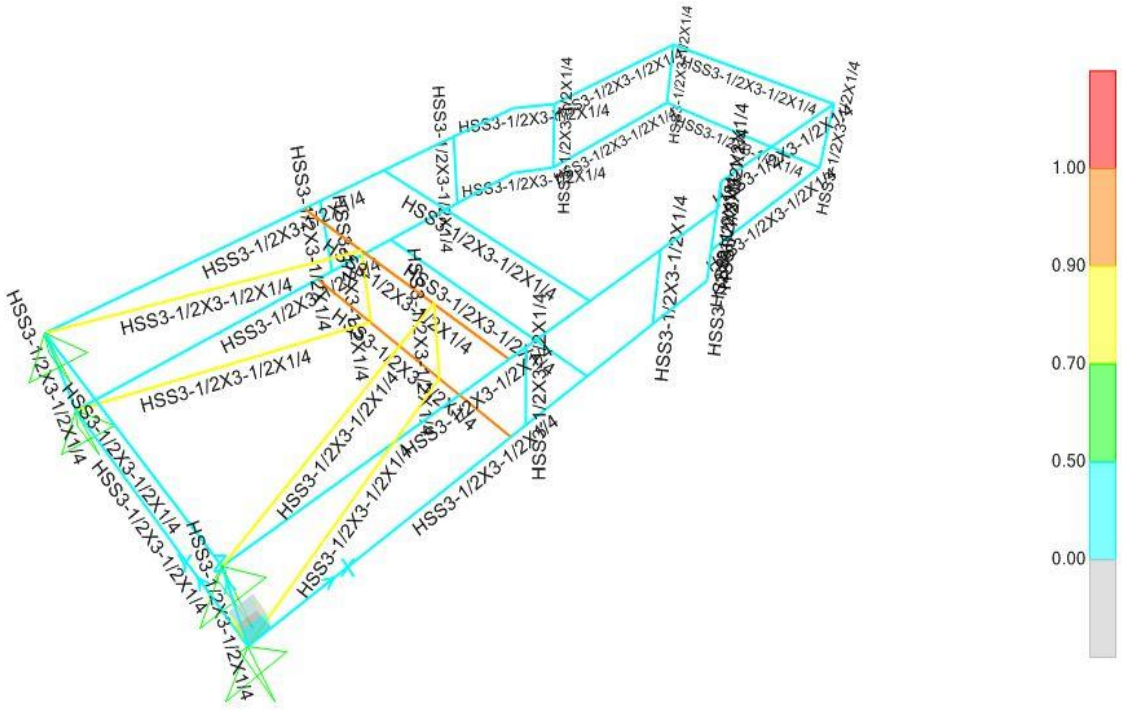

Figure V.12: Stress Checks of Steel Frame Calculated using Sap 2000 Model.

It can be seen by the color coding in Figure V.12, the cross-members, where the linear compression spring system is connected, has the highest utilization of the

available resistance provided by the structural member. This member has a utilization ratio of 0.906 for the member with shear as the limiting load case. Since this member is less than 1.00 the member is suitable for this design.

Summary

This section discussed the design of a linear compression spring system and a structural frame for the Low Speed Surrogate Vehicle. The linear compression springs were determined to have the stiffness of 620 lbs/in when the displacement is from 0 - 20 inches, 8,125 lbs/in from 20 - 32 inches, and from 32 - 44 inches, a 399 psi honeycomb material should be used with dimensions of 13.5 x 21.0 inches. This provides a constant force of approximately 110 kips. A single degree of freedom dynamic analysis was performed on the linear compression spring system to ensure that the springs were adequately designed. The combination of linear compression springs and honeycomb material should act through the center of gravity of the surrogate vehicle. This is to reduce any eccentric loading unaccounted for in the design process.

A structural frame was necessary to contain the force produced by the linear compression spring system. This structural frame was designed with HSS 3.5 x 3.5 x 0.25 Grade 50 tubes. The structural frame was designed and validated using Sap 2000. Figure V.12 shows the utilization ratio of the resistance provided by the steel tubing. These members were acceptable when loaded to the extreme loading of 115 kips with a dynamic load factor of 2.0. This increases the total load to 230 kips of load transferring through the structural frame. The increase in the load was to ensure that the frame does not yield and can withstand the continued loading of 115 kips with minimal maintenance

to the structural frame. Detailed design drawings for the proposed surrogate vehicle can be found in Appendix B.

CHAPTER VI

DYNAMIC FINITE ELEMENT ANALYSIS OF SURROGATE VEHICLE

After the design of the Low Speed Surrogate Vehicle was complete, it was necessary to validate the overall effectiveness of this vehicle. For the purpose of this research, two programs were used to model the surrogate vehicle: Hypermesh version 12.0 and LS-DYNA (Altair HyperWorks 2014) (LSTC 2014). Hypermesh was used to create and modify the finite element model which will then be computed by LS-DYNA, a non-linear finite element program (Altair HyperWorks 2014) (LSTC 2014). In this program the finite element model was created by assigning a particular mesh, material properties, and contact requirements to each component. This information was then exported into a file that was compatible with LS-DYNA (LSTC 2014). Two key aspects of the Low Speed Surrogate Vehicle were analyzed for their overall effectiveness. These two components were the global force-deformation response and the structural capacity of the frame. This chapter will discuss the overall process of creating and analyzing the results of the finite element model of the Low Speed Surrogate Vehicle.

Development of Finite Element Models

There are several steps in simulating a full-scale crash test in a finite element program. Becker *et al.* (1981) states that there are three key parts to any finite element model. These three parts are the preprocessor, processor, and postprocessor (Becker 1981). In the preprocessor, the finite element model and any necessary properties and contacts between the components are established. The processor is where the finite

element model is computed. This step can be very time consuming depending on the size of the model and its properties. The postprocessor allows the modeler to view and analyze the results, providing the opportunity to look at key pieces of the model to determine the adequacy of the components. In this research, two programs were used to create, compute, and analyze the finite element models. Hypermesh was used as the preprocessor (Altair HyperWorks 2014). This was decided due to the ease of creating and editing the finite element models. LS-DYNA, on the other hand, was used as the processor (LSTC 2014). LS-DYNA is widely used in the crash testing community and was therefore selected as the processor for this application (LSTC 2014). For the postprocessor, LS-Prepost was utilized (LSTC 2014). LS-Prepost is a program that is a subset of LS-DYNA but specifically used to create graphics and analyze components from the finite element simulation (LSTC 2014). LS-Prepost can also be used to make modifications to the finite element model (LSTC 2014).

To make the finite element models discussed herein, three different types of elements were utilized. These elements are shell elements, solid brick elements, and discrete spring elements. The first two types of elements can be seen in Figure VI.1. Shell elements use four nodes which are all aligned within a 2D plane. Solid brick elements use eight nodes and are 3D elements. These elements were utilized based on the geometry and material type of the object being modeled. To reduce the computation time, a single discrete spring element was used to model the linear compression spring system of the Low Speed Surrogate Vehicle. A discrete spring element uses two nodes as end nodes and regulates the force-deformation relationship between these nodes. To

reduce the overall size and the computation time of the models, shell and discrete elements were used wherever possible.

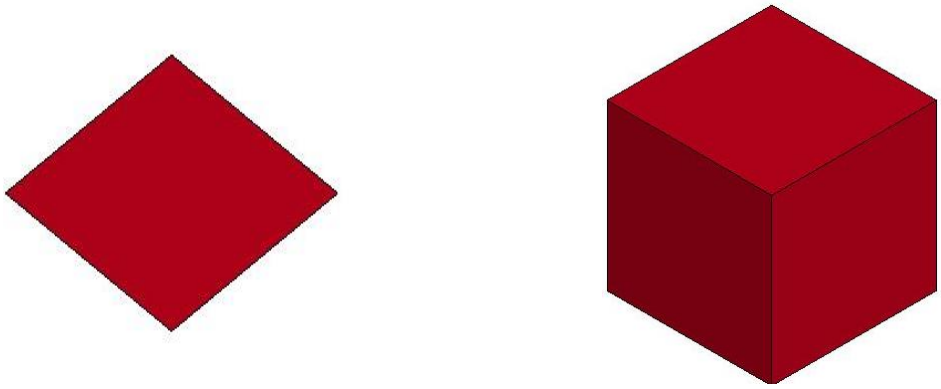

Figure VI.1: Different Types of Elements used in the following Finite Element Models: (a) Shell Element, (b) Solid Brick Element.

Non-Linear Spring and Mass Model

A basic finite element model of a spring attached to a 5,000 lbs weight was created to ensure that accurate results were being obtained from LS-DYNA (LSTC 2014). This model was created to compare, the single degree of freedom dynamic model discussed in Chapter IV. Since this discrete spring element uses only one spring with different stiffness, LS-DYNA considers this element to be a non-linear spring element; although in reality, this would be achieved using a series of linear compression springs and honeycomb material acting at specific intervals (LSTC 2014). Figure VI.2 shows the non-linear spring and mass model created in LS-DYNA (LSTC 2014).

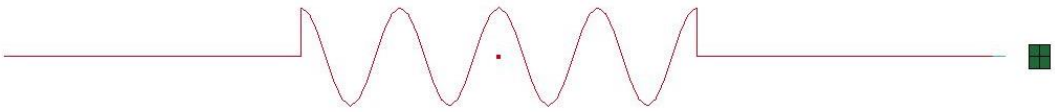

Figure VI.2: Display of the Non-Linear Spring and Mass Model.

As mentioned earlier, the weight of the block, located on the right hand side of Figure VI.2, is 5,000 lbs. The block was assigned a rigid material card. Using this card allowed for a Constrained Extra Node to be assigned to this block. This node will move rigidly with the block. The extra node was then used to tie the non-linear discrete spring element to the rigid block. The other end of the discrete spring was held fixed in all directions (laterally, vertically, horizontally, and all three rotational degrees). The discrete spring was given a material card of S08 in LS-DYNA (LSTC 2014). S08 is a non-linear, inelastic spring material card which allows the spring to compress without rebounding. This is a necessary trait to have built into the surrogate vehicle finite element model because *ASTM F3016* (2014) requires the surrogate vehicle to contain the spring force after the completion of the test. Containing the spring force is required to prevent the protective device from seeing additional load after the completion of the test and to prevent the surrogate vehicle from rebounding. The S08 material card requires a force-deformation curve to be provided as a part of the material card. A force-deformation curve was created using the optimized spring stiffness and can be seen in the single degree of freedom dynamic results found in Chapter IV. An initial velocity of 30 mph was imposed on the rigid block. The 30 mph speed was selected to reflect the

maximum speed of the surrogate vehicle when used in a full-scale crash test. The results of this model are discussed later in this chapter.

Surrogate Vehicle Validation Model

To test the effectiveness of the Low Speed Surrogate Vehicle, a finite element model of the vehicle was created in Hypermesh (Altair HyperWorks 2014). This model utilizes shell, solid brick, and discrete spring elements to define different components of the surrogate vehicle. Shell elements were used to represent anything with a constant thickness such as structural tubing or solid plates. Solid brick elements were used to represent the rubber pad attached to the front of the nose of the surrogate vehicle model. This element type was selected because of the large deformations and stresses experienced in the material during impact.

This model also uses a discrete non-linear inelastic spring element to model the linear compression spring system. This element uses the force-deformation curve provided by the single degree of freedom dynamic model. The surrogate vehicle model assumes that the linear compression spring system is confined solely within the impacting direction of the vehicle. This constraint of the spring system was assumed because the surrogate vehicle utilizes a series of pipes to confine the motion of the linear compression spring system to be only in the impacting direction. The same S08 material card was used in the surrogate vehicle model and the non-linear spring and mass model. Material properties were then assigned to every element used within the surrogate vehicle model. The properties were assigned to each part as specified in the design drawings found in Appendix B. Within surrogate vehicle model, many different

material cards were used to represent the different material properties of the different components. In LS-DYNA MAT_001 Linear Elastic, MAT_020 Rigid, and MAT_024 Piecewise, Linear Plasticity material cards were a few of the material cards used within this model (LSTC 2014). The final surrogate vehicle model can be seen in Figure VI.3.

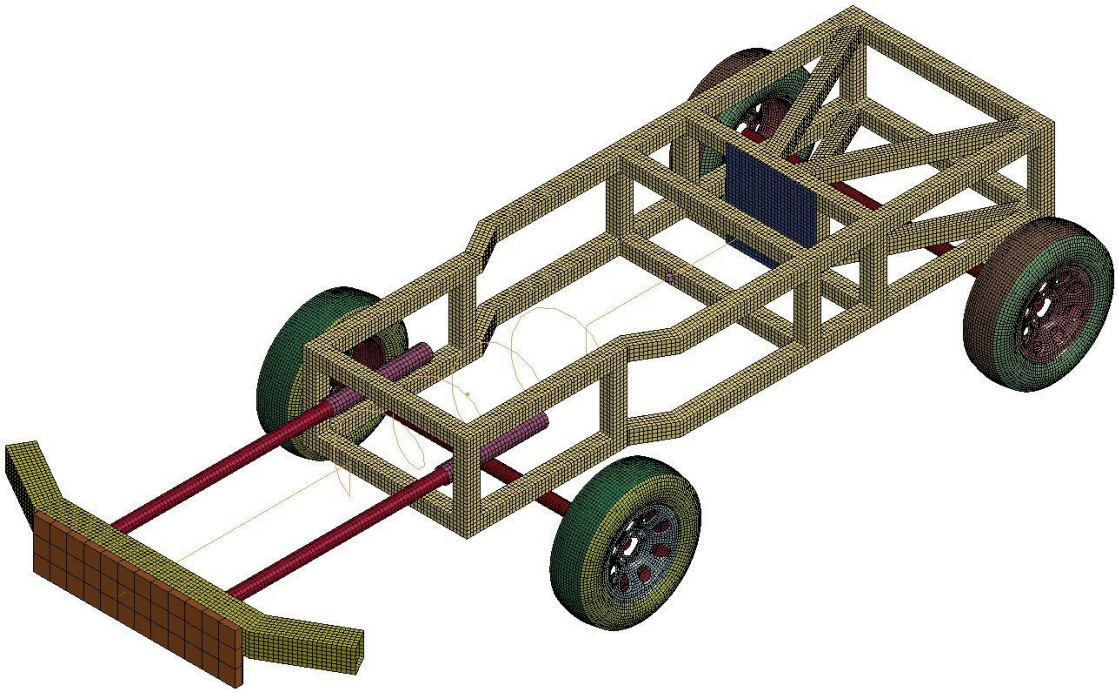

Figure VI.3: The Final Surrogate Vehicle Model as seen in LS-DYNA (LSTC 2014).

Only one contact card was used in the finite element model of the surrogate vehicle. This contact card was the Automatic Surface to Surface contact card. This keeps any component from passing through another component of the vehicle. Items such as the rubber bumper pad, the sweeper plate, and impactor nose were tied together using Constrained Nodal Rigid Bodies where the bolts would connect the pieces together.

One additional component was added to the surrogate vehicle that is incorporated in the design drawings found in Appendix B. This component is a single, rigid solid brick element that is used to gather the accelerations at the center of gravity of the vehicle. In a full-scale test, this block would be where an accelerometer would likely be placed in order to capture the global behavior of the surrogate vehicle.

For this model, the bumper of the surrogate vehicle is held fixed in all directions. Since the bumper is set forth in the *ASTM F3016* (2014) standard, it was determined this component was not a critical component of the surrogate vehicle design. Therefore this component was rigidly fixed to remove any adverse effects experienced by this component. Future testing should be performed to ensure that this assumption is valid. Additionally, everything was given an initial velocity of 30 mph. The maximum speed of 30 mph is the highest initial test velocity stated in *ASTM F3016* (2014).

Finite Element Model Results

After the completion of the finite element simulations, the following results were obtained from LS-DYNA (LSTC 2014). These results were then compared to the measured values from the Baseline 30 mph Pickup Truck Test and from the single degree of freedom dynamic analysis of the surrogate vehicle.

Non-Linear Spring and Mass Model Results

The results of the non-linear spring and mass model are shown below. Figure VI.4 displays the velocity vs time graph of the single degree of freedom (SDOF) dynamic model and the finite element analysis. Figure VI.5 shows the force-

deformation response for both sets of data. It can be determined that the non-linear inelastic discrete spring material card used to define the stiffness of the spring adequately models the linear compression spring system used in the Low Speed Surrogate Vehicle design. Figure VI.6 shows a comparison between the force vs time curve of the finite element model and the single degree of freedom dynamic model with equally adequate results.

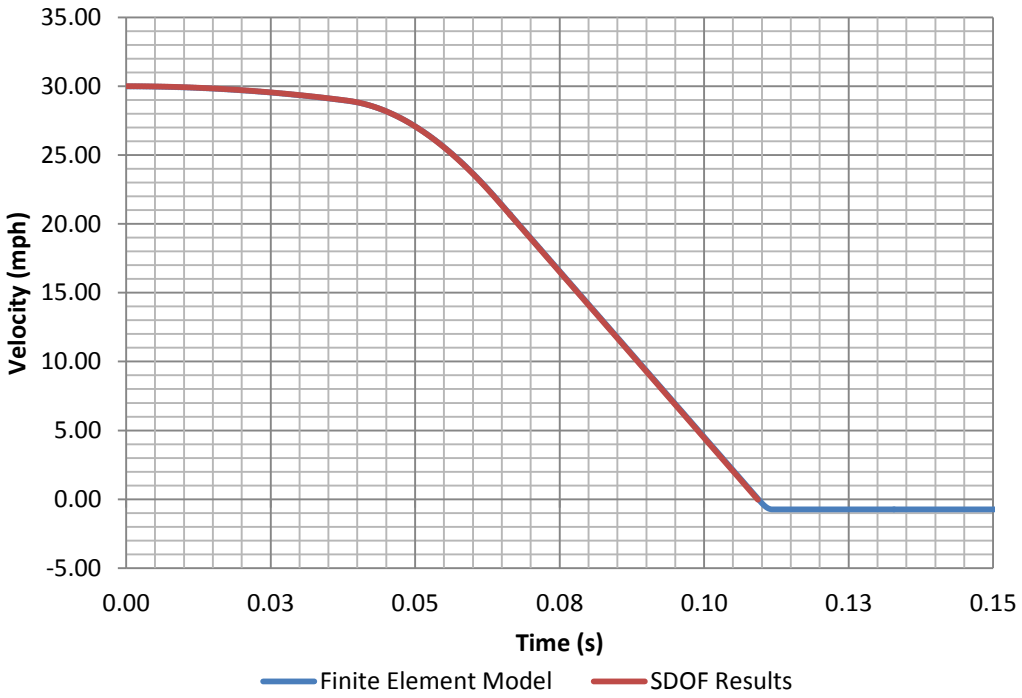

Figure VI.4: Velocity vs Time Comparison between a SDOF Dynamic Model and a Non-Linear Inelastic Spring Model.

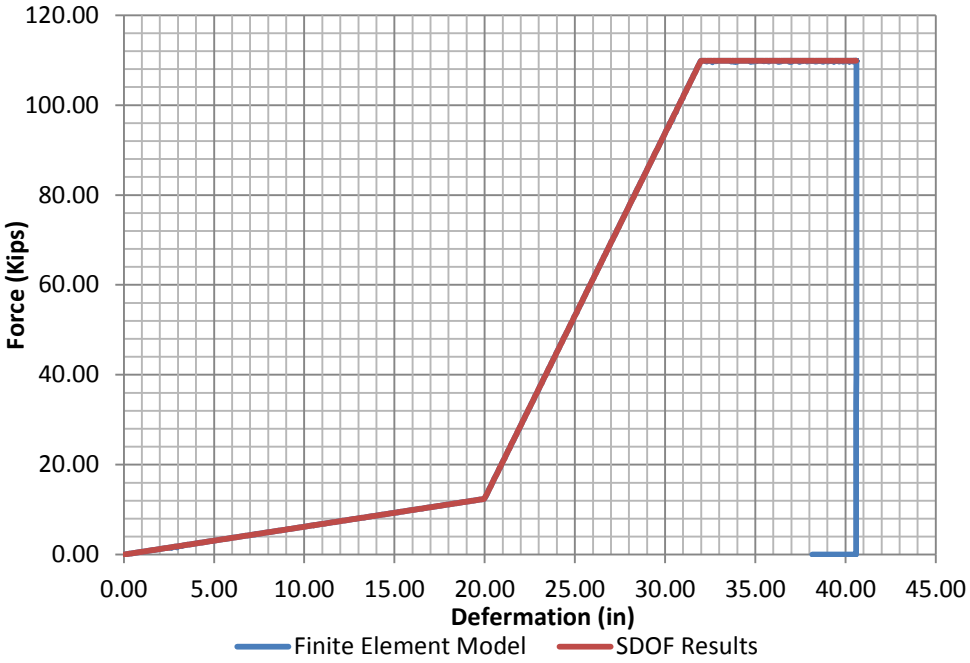

Figure VI.5: Force vs Deformation Comparison between a SDOF Dynamic Model and a Non-Linear Inelastic Spring Model.

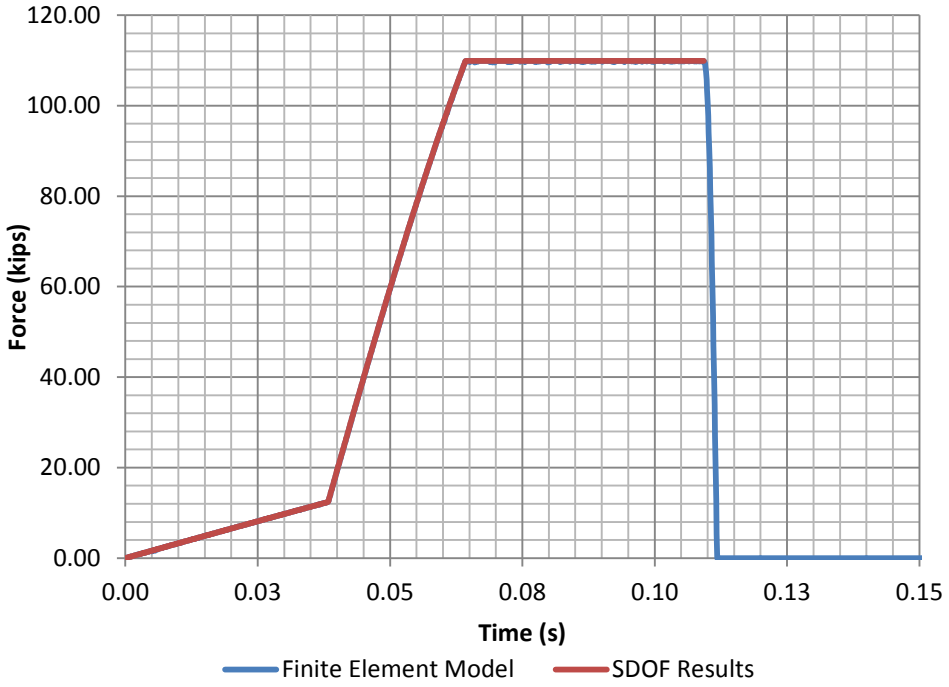

Figure VI.6: Force vs Time Comparison between a SDOF Dynamic Model and a Non-Linear Inelastic Spring Model.

Surrogate Vehicle Validation Model Results

The results of the surrogate vehicle finite element model is compared to the full-scale crash test of the 2005 Dodge Ram 1500 pickup truck described in Chapter IV and the single degree of freedom (SDOF) dynamic analysis discussed in Chapter V. The results are divided into two different categories: Global Force-Deformation Results and the Structural Capacity of Surrogate Vehicle Frame Results.

Global Force-Deformation Results

The purpose of this section was to validate the global force-deformation response of the surrogate vehicle. This curve is predicted to resemble the force-deformation response of the test vehicle captured in the full-scale crash test expressed in Chapter IV.

Figure VI.7 shows the velocity vs time graph of the SDOF dynamic model and the finite element analysis of the surrogate vehicle. Figure VI.8 shows the force vs time relationship between the single degree of freedom dynamic model and the finite element analysis. There is a slight difference between these two graphs. This is due to the differences between the stiffness of the test vehicle and the idealized vehicle stiffness. Figure VI.9 shows the force-deformation response of the single degree of freedom, the finite element analysis, and the results of the full-scale crash test. From this figure, it can be seen that the force-deformation graphs of the dynamic analysis and the finite element match with little to no deviations.

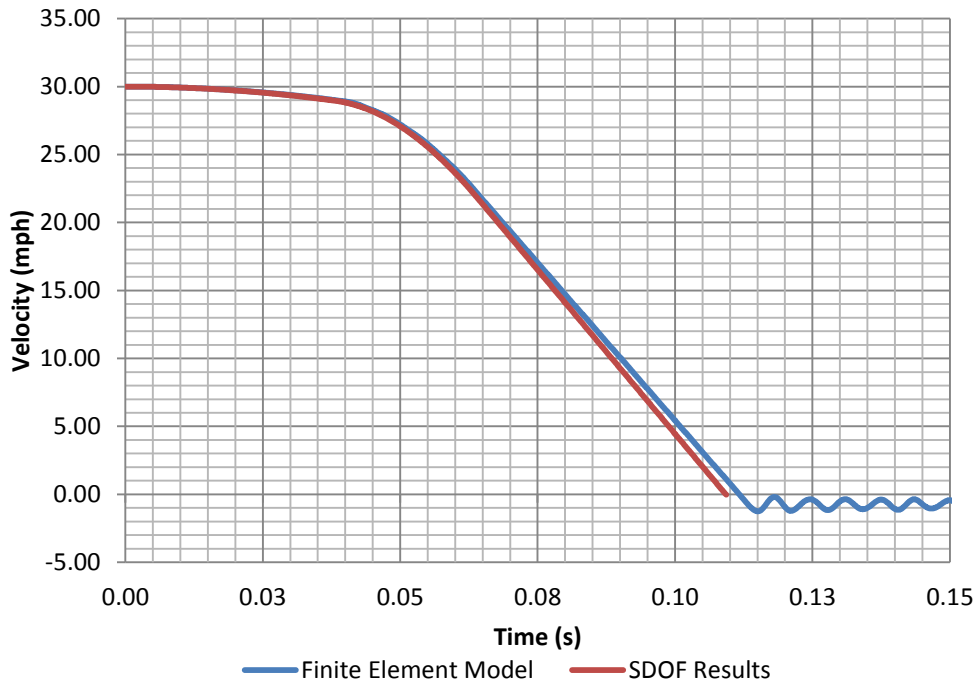

Figure VI.7: Velocity vs Time Graph showing the Difference between the Finite Element Results and the SDOF Results.

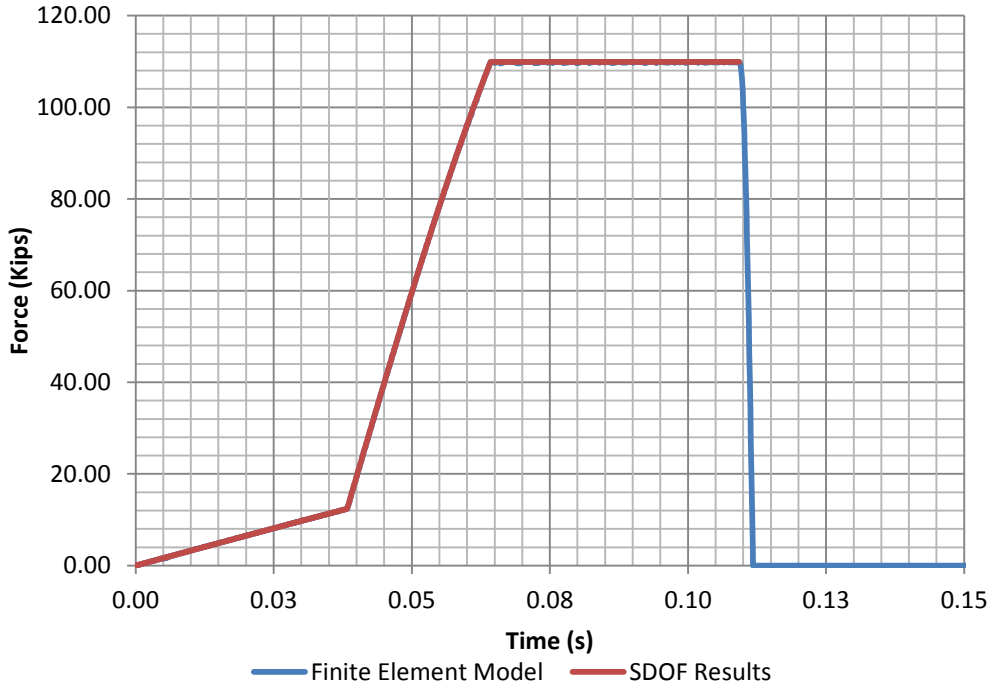

Figure VI.8: Force vs Time Graph showing the Difference between the Finite Element Results and the SDOF Results.

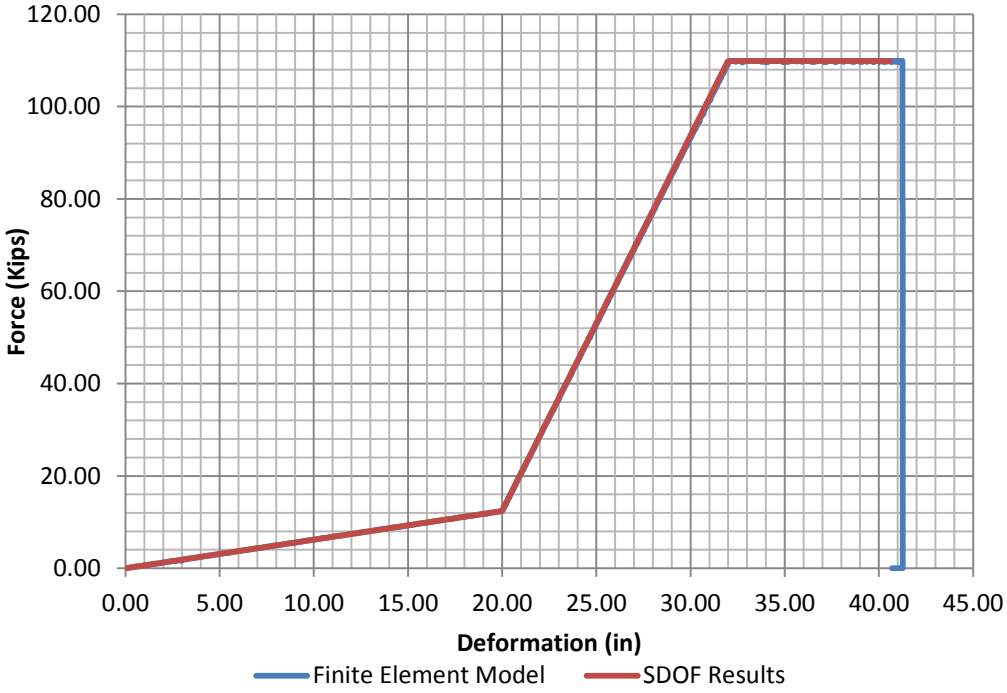

Figure VI.9: Force-Deformation Relationship showing the Differences between the Finite Element Results, SDOF Results, and the Full-Scale Crash Test Results.

Structural Capacity of Surrogate Vehicle Frame Results

The structural frame was designed using a static finite element model, Sap 2000. In this model the largest force experienced by the full compression of the ASTM springs was then amplified by a dynamic load factor of 2.0. This load was then applied statically to the frame using distributed loads applied to the contacting members. To verify the adequacy of the frame, the stresses were analyzed using the surrogate vehicle finite element model shown in Figure VI.3. The frame was designed in a manner so that the yielding stress of the material would never be reached. Figure VI.10 shows the stresses found within the frame. These stresses were limited between the range of zero and the yield stress of the material. It can be seen that most of the frame has used a small amount of the total capacity found in the members. The maximum amount of stress experienced by the structural frame during the test is approximately 25% of the yield stress.

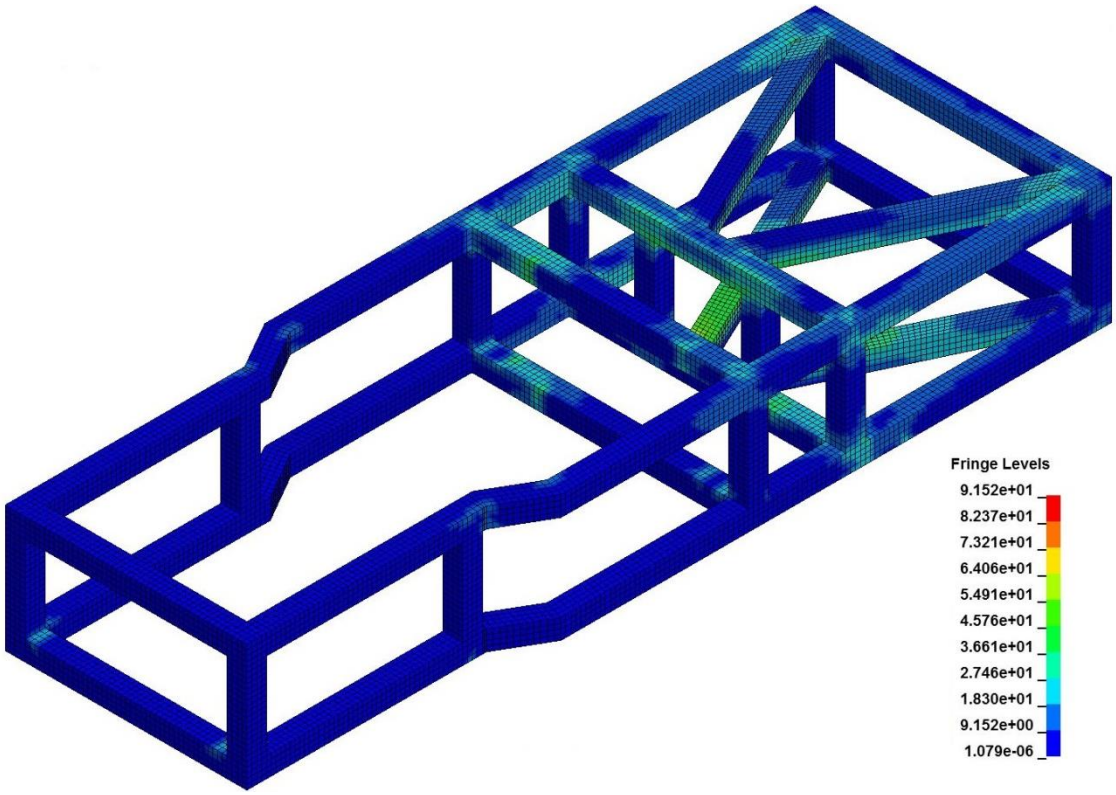

Figure VI.10: Von Mises Stresses within the Surrogate Vehicle Frame Limited by the Yielding Stress of the Material.

As a result, the frame was shown to be adequately designed to withstand the forces experienced during a full-scale crash test. It was also determined that the dynamic load factor of 2.0 was significantly high for this application and should be reduced in future applications similar to the type of loading expressed here.

Summary

LS-DYNA was used to compute the non-linear finite element model of the Low Speed Surrogate Vehicle (LSTC 2014). A single degree of freedom dynamic model was created to ensure that the results obtained from LS-DYNA were accurate but also so that they can be explained (LSTC 2014). With this knowledge, a non-linear inelastic spring

analysis was created to ensure that the material card of the inelastic spring was accurately modeled. Using this knowledge a finite element model of the surrogate vehicle model was created in LS-DYNA (LSTC 2014). The force-deformation response was verified using the single degree of freedom dynamic analysis. The frame was also examined to see if any members reached the yielding limit, and since no member reached this point, we can be assured that no plastic deformation would form within this structure.

CHAPTER VII

CONCLUSIONS AND RECOMMENDATIONS

Every day people use automobiles to travel to and from work, the store, or to complete their daily routine. With 60 automotive accidents occurring daily that involve storefronts, the need for having protective devices tested and implemented is increasing (Storefront Safety Council 2015). To ensure that these devices will perform adequately, *ASTM F3016* (2014) standardized a test method to validate these devices. This standard requires the use of a surrogate vehicle in the testing of the protective device. *ASTM F3016* (2014) does not specifically define the surrogate vehicle to be used in this type of testing. Therefore the primary objective of this thesis was to design and validate a reusable test vehicle to be used in full-scale crash tests of protective devices rated by *ASTM F3016* (2014).

To assist in designing the surrogate vehicle, a full-scale crash test of a 2005 Dodge Ram 1500 pickup truck was tested by TTI (Brackin, Menges 2014). This test was conducted to both *MASH 2270P* (AASHTO 2009) and *ASTM F3016* (2014) standards. The data from this test were used to design the force-deformation response and the structural frame of the surrogate vehicle.

In general, the surrogate vehicle has general characteristics resembling a *MASH 2270P* (AASHTO 2009) pickup truck along with the critical dimensions specified by *ASTM F3016* (2014). The critical characteristics of this vehicle were the gross static vehicle weight, the height to the center of gravity, and the force-deformation response.

The force-deformation of the surrogate vehicle was achieved by using a series of linear compression springs. The spring stiffness are set by *ASTM F3016* (2014) to be 620 lbs/in from 0 - 19 inches, 8,125 lbs/in from 19 - 31 inches, and a constant 110 kips from 31 - 41 inches. The stiffness of these springs deviate from the full-scale tests shown in Figure IV.13. It was seen that the data collected by TTI were not accurately described by the *ASTM F3016* (2014) spring stiffness. Using the least squares optimization principles, optimum spring stiffnesses have been determined. These stiffnesses were found to be 620 lbs/in from 0 - 20 inches, 8,125 lbs/in from 20 - 32 inches, and a constant 109.9 kips from 32 - 44 inches. Although the spring rates remained fairly constant, the intersection point of the two spring rates changed. Figure IV.15 shows the comparison between the spring stiffness set by *ASTM F3016* (2014), the vehicle stiffness of a 2005 Dodge Ram 1500 pickup truck captured by TTI (Brackin, Menges 2014), and the optimized spring stiffness determined by using least squares optimization.

A structural frame was designed using a maximum force of 115 kips, which was the maximum force captured by the full-scale test of the 2005 Dodge Ram 1500 pickup truck (Brackin, Menges 2014). A dynamic load factor of 2.0 was applied to ensure that no yielding was achieved within the structural frame. Using the non-linear finite element analysis program, the frame was found to remain significantly below the threshold of yielding.

From the non-linear finite element models and the single degree of freedom dynamic analysis discussed earlier, the Low Speed Surrogate Vehicle will accurately model the impact of a *MASH 2270P* (AASHTO 2009) pickup truck traveling 30 mph or

less and impacting a protective device. However before any product testing is completed, it is recommended that the surrogate vehicle is verified by performing a full-scale crash test into a rigid object. Upon receiving amicable results, the surrogate vehicle can be used to test any form of protective device to the *ASTM F3016* (2014) standard, and finally it is recommended that this surrogate vehicle design be incorporated into the *ASTM F3016* (2014) standard.

Protective devices need to meet two key areas to control the issues of vehicular accidents with vulnerable objects. The first aspect is to make sure that the device can control the errant vehicle. The second key area is the cost of the protective device. Although the cost of each protective device is only controlled by the supplier, the cost of the full-scale testing was attempted to be reduced to save the consumer money. The surrogate vehicle designed in this thesis will allow for test facilities to easily validate the worthiness of the protective devices while also reducing the overall cost of the full-scale crash test.

REFERENCES

Altair HyperWorks. (2014). *Hypermesh Version 12.0*. Retrieved March 23, 2015, from Altair Hyperworks: http://www.altairhyperworks.com/hwhelp/Altair/hw12.0/help/hm/hmbat.aspx

American Association of State Highway and Transportation Officials (AASHTO). (2009). *Manual for Assessing Safety Hardware.* Washington, D.C.: AASHTO.

American Institute of Steel Constructuion. (2013). *Steel Construction Manual 14th Edition.* United States of America: American Institute of Steel Constructuion.

ASTM International. (2007). *ASTM F2656 - Standard Test Method for Vehicle Crash Testing of Perimeter Barriers.* West Conshohocken: ASTM International.

ASTM International. (2014). *ASTM F3016 - Surrogate Testing of Vehicle Impact Protective Devices at Low Speeds.* West Conshohocken: ASTM International.

Becker, E. B., Carey, G. F., & Oden, J. T. (1981). *Finite Element An Introduction Volume 1.* Austin: The University of Texas at Austin.

Biggs, J. M. (1964). *Introduction to Structural Dynamics.* New York, San Francisco, Toronto, London: McGraw-Hill Book Company.

Brackin, M. S., & Menges, W. L. (2014). *2005 Dodge Ram 1500 Pickup Truck into Semi-Rigid Pier.* College Station: Texas A&M Transportation Institute.

City of Artesia. (2014). *City Council Agenda Report.* City of Artesia: City of Artesia.

Dawson, H., & Tennant, D. (2008). Inelastic Dynamic Finite-Element Design of Bollard Systems to Impact Loading. *ASCE Structures Congress*.

Desorcie, F. J., Alberson, D. C., & Reiter, R. (2013). Data Analysis and Prevention of Vehicle-Into-Building Crashes.

Emori, R. I. (1968). Analytical Approach to Automobile Collisions. *Society of Automotive Engineers*.

Hott, C., Brown, C., & Totani, N. (1990). *Crush Characteristics of the 1800 lb Pendulum.* McLean: United States Department of Transportation Federal Highway Administration.

Hott, C., Brown, C., Totani, N., & Hansen, A. (1990). *Crush Characteristics of the "Breakaway" Bogie.* McLean: United State Department of Transportation Federal Highway Administration.

Hu, B., Li, G., Chen, S., & Shi, W. (2011). State-of-the-Art Review on Anti-ram Bollards. *Applied Mechanics and Materials*, 3206-3213.

Keske, M., Brown, A., Brennan, S., & Qiu, T. (2014). Low-order Modeling of Vehicle Impacts upon Boulders Embedded in Cohesionless Soil. *International Journal of Impact Engineering*, 88-99.

Liu, C., Phang, S. K., & Sun, J. (2009). Effect of Site Conditions on the Design of Removable Anti-Ram Bollards. *Key Engineering Materials*, 801-805.

Livermore Software Technologt Corperation (LSTC). (May 26, 2014). *LS-DYNA Keyword User's Manual Volume 1.* Livermore: LSTC.

Livermore Software Technology Corperation (LSTC). (May 19, 2014). *LS-DYNA Keyword User's Manual Volume 2.* Livermore: LSTC.

Miami-Dade County. (2012, April 27). Zoning Amending Plan Review Standards in Business Districts. Miami-Dade County, Florida.

Society of Automotive Engineers. (2007). *Surface Vehicle Recommended Practive S J211*. United States of America: Society of Automotive Engineers.

Storefront Safety Council. (2014, November 12). Retrieved from Storefront Safety Council: www.storefrontsafety.org

Texas A&M Transportation Institute. (2013, June 13). *Simulated Crash Testing Saves Time and Money*. Retrieved March 2015, from Texas A&M Transportaiton Institute: http://tti.tamu.edu/2013/06/13/simulated-crash-testing-saves-time-and-money/

Wright, C. (2012). *Introduction to Structural Impact.* Fairfax, VA: PDH Online.

APPENDIX A

BASELINE 30 MPH PICKUP TRUCK TEST

Additional Data from Baseline 30 mph Full-Scale Crash Test

Additional data collected from the full-scale crash testing of the 2005 Dodge Ram 1500 into an instrumented simulated bollard is shown below. A test vehicle's properties data sheet is included in Table A.1(Brackin, Menges 2014). Figure A.1 shows a summary of the test vehicle and its progression through the entire event (Brackin, Menges 2014). Figure A.2 shows the longitudinal accelerations collected by the lower accelerometer (Brackin, Menges 2014). Figure A.3 shows the longitudinal accelerations collected by the accelerometer located at the center of gravity of the simulated bollard (Brackin, Menges 2014). Figure A.4 shows the longitudinal accelerations collected by the upper accelerometer (Brackin, Menges 2014). Figure A.5 shows the longitudinal accelerations collected by the accelerometer located at the center of gravity of the test vehicle (Brackin, Menges 2014). Figure A.6 shows the lateral accelerations collected by the accelerometer located at the center of gravity of the test vehicle (Brackin, Menges 2014). Figure A.7 shows the vertical accelerations collected by the accelerometer located at the center of gravity of the test vehicle (Brackin, Menges 2014).

Table A.1: Test Vehicle Properties (Brackin, Menges 2014)

Date: 2013-09-13 Test No.: 194001-USD1 VIN No.: 1D7HA18D355520813

Year: 2005 Make: Dodge Model: Ram 1500

Tire Inflation Pressure: 35 psi Odometer: 175724 Tire Size: 245/70R17

Describe any damage to the vehicle prior to test:

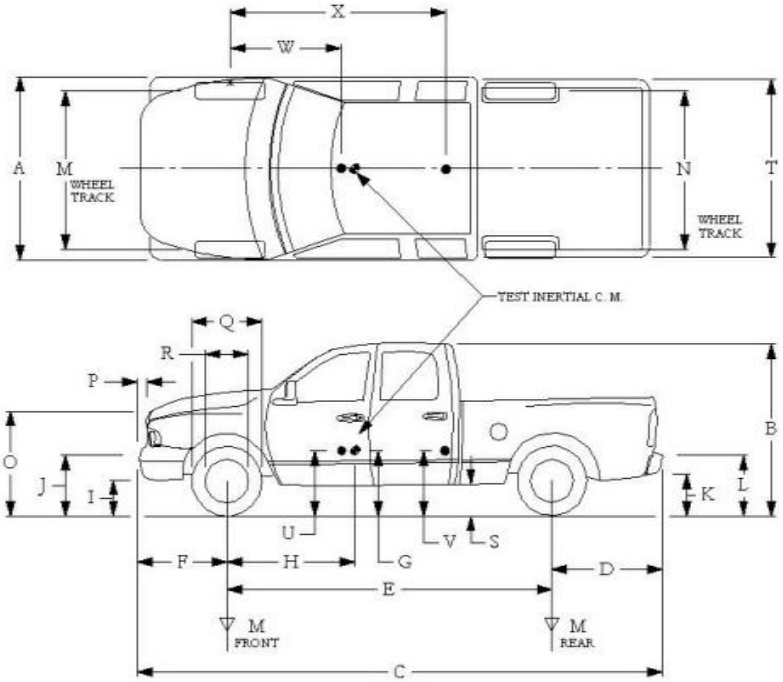

- Center of Mass
- Accelerometer

Geometry: inches

A	77.00	F	39.00	K	20.50	P	3.00	U	28.00
B	73.25	G	28.12	L	28.75	Q	29.50	V	33.00
C	227.00	H	64.05	M	68.25	R	18.50	W	64.00
D	47.50	I	13.50	N	67.25	S	14.25	X	160.00
E	140.50	J	26.00	O	44.75	T	75.50		

Mass Distribution:

lbs LF: 1379 RF: 1351 LR: 1157 RR: 1130

Mass: lbs	Curb	Test Inertial	Gross Static
M_{front}	2762	2730	
M_{rear}	1993	2287	
M_{Total}	4755	5017	

0.000 s

0.121 s

0.242 s

0.363 s

Before Test

Before Test

After Test

After Test

General Information

Test Agency	Texas A&M Transportation Institute
Test Standard Test No.	*ASTM F2656-07* PU30
Test No.	194001-USD1
Date	2013-09-13

Test Article

Type	Security Barrier - Bollard
Name	Simulated Bollard/Instrumented Pier
Installation Dimensions	10-inch diameter bollard attached to 36-inch diameter x 14 ft tall pier
Material or Key Elements	Simulated bollard on simulated steel bridge pier supported by braced column load frame and foundation system
Soil/Foundation Type	Concrete footing in crushed limestone

Test Vehicle

Type	Pickup
Designation	PU30
Model	2005 Dodge Ram 1500 Pickup
Mass	
Curb	4755 lb
Test Inertial	5017 lb

Impact Conditions

Speed	30.5 mi/h
Angle	90 degrees

Exit Conditions

Speed	Stopped
Angle	90 degrees

Occupant Risk Values

Impact Velocity	
Longitudinal	46.2 ft/s
Lateral	0.7 ft/s
Ridedown Accelerations	
Longitudinal	3.7 G
Lateral	3.0 G
Max. 0.050-s Average	
Longitudinal	-23.2 G
Lateral	-1.8 G
Vertical	-8.5 G

Penetration of Cargo Bed

Distance Beyond Inside Edge of Security Device	Did not penetrate
Was Vehicle Disabled?	Yes

Figure A.1: Summary of Results for the Baseline 30 mph Pickup Truck Test into a Simulated Bollard (Brackin, Menges 2014).

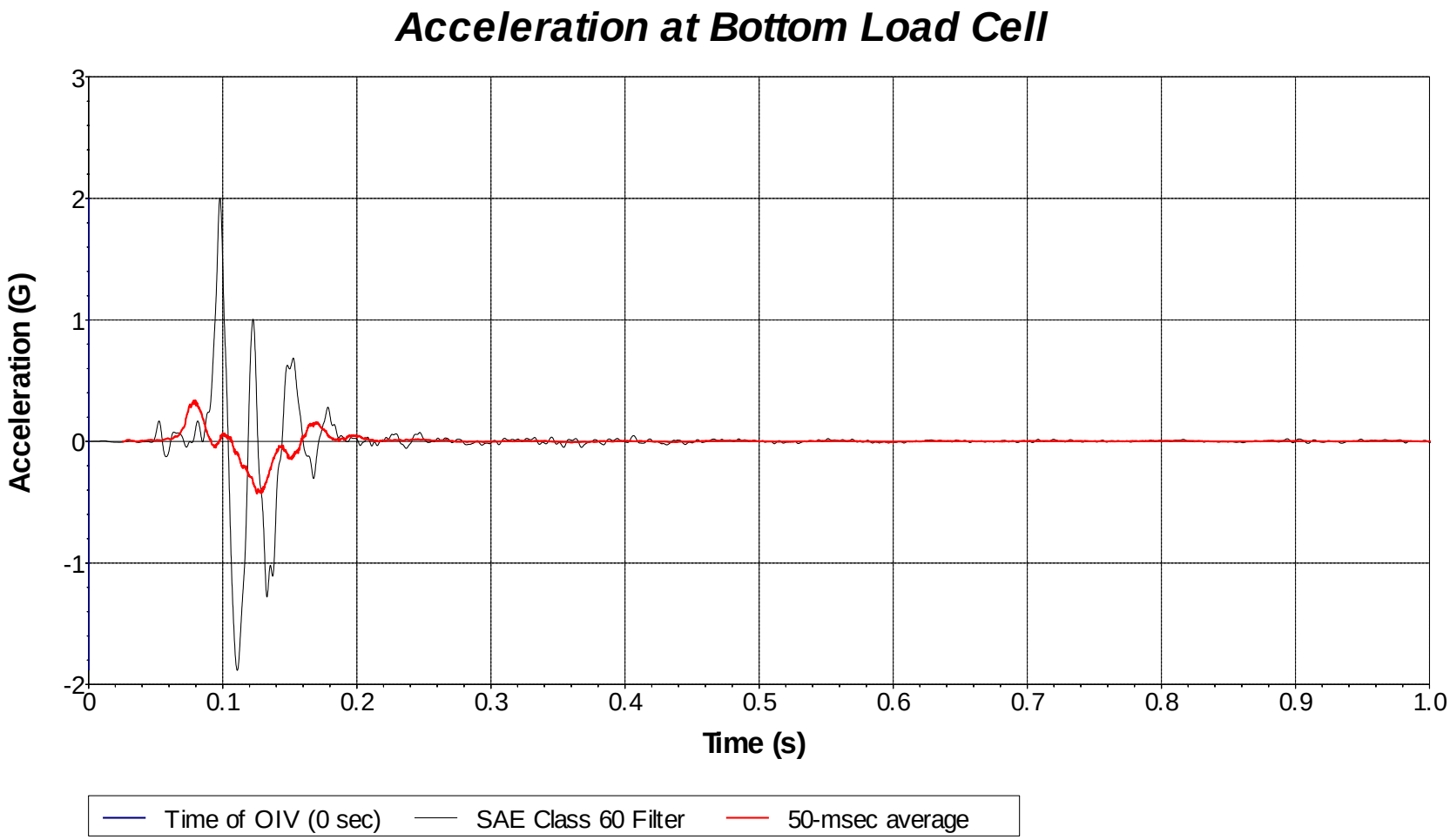

Figure A.2: Longitudinal Acceleration 24 inches from Base of Instrumented Pier (Brackin, Menges 2014).

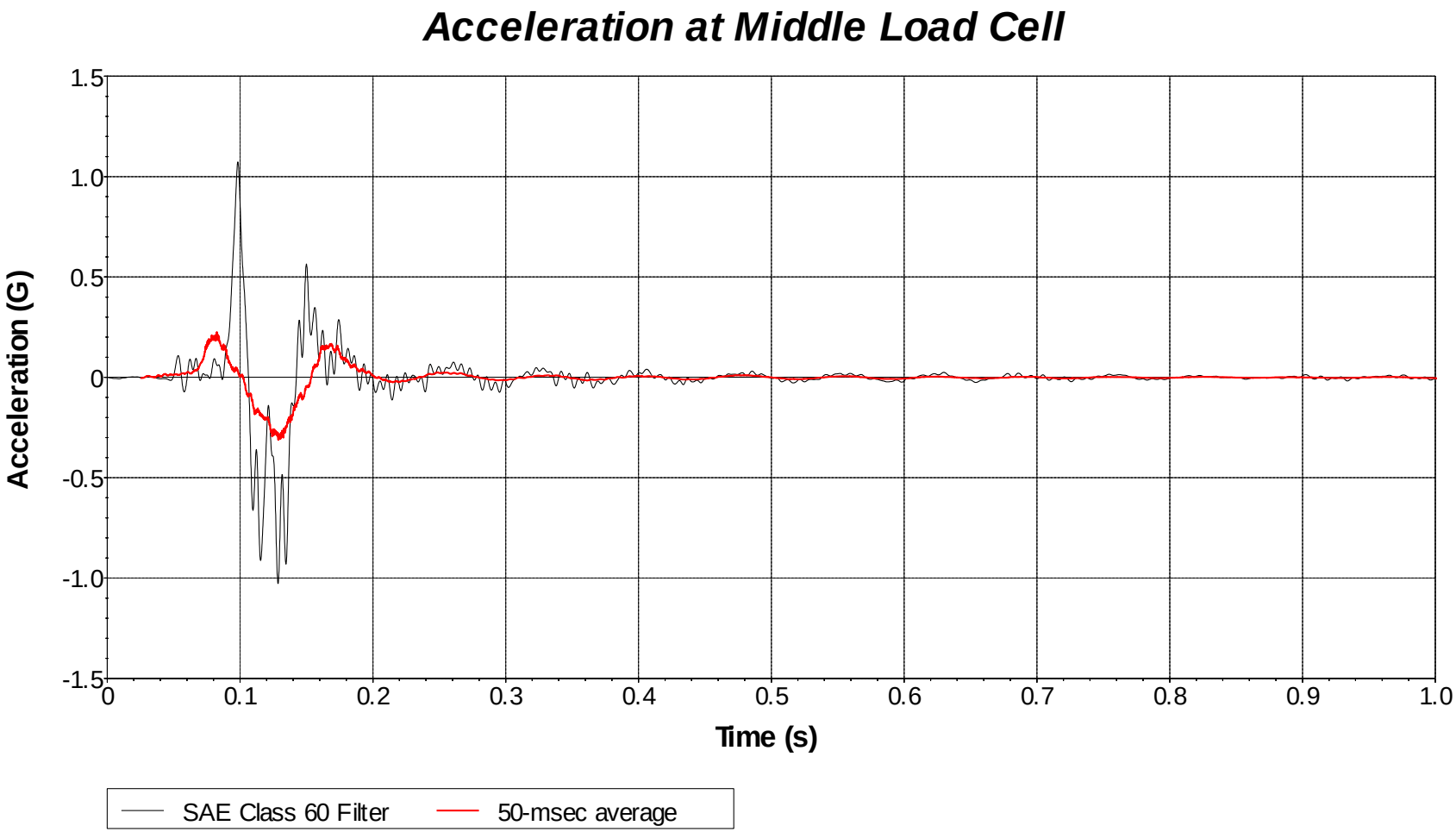

Figure A.3: Longitudinal Acceleration 84 inches from Base of Instrumented Pier (Brackin, Menges 2014).

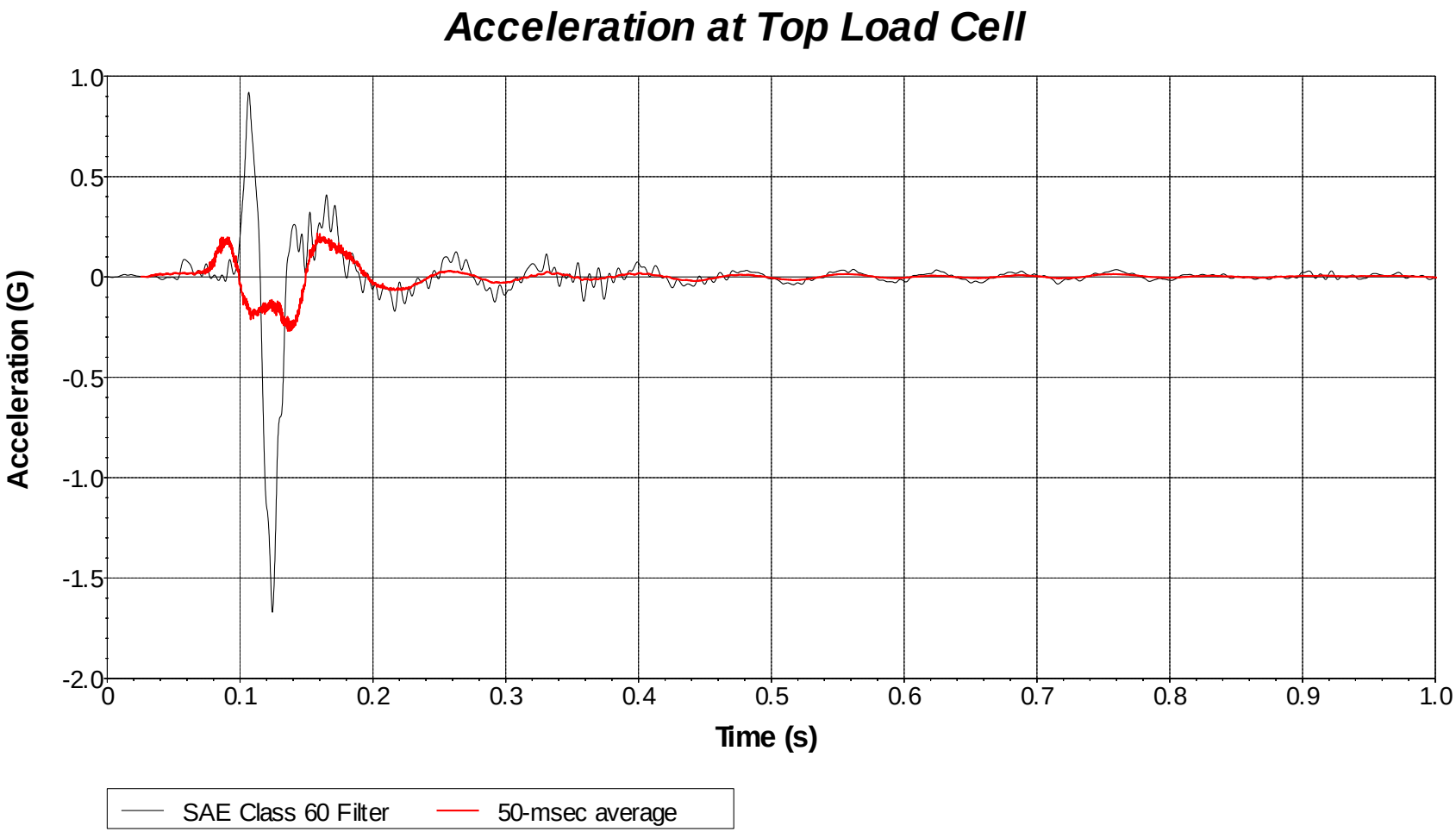

Figure A.4: Longitudinal Acceleration 144 inches from Base of Instrumented Pier (Brackin, Menges 2014).

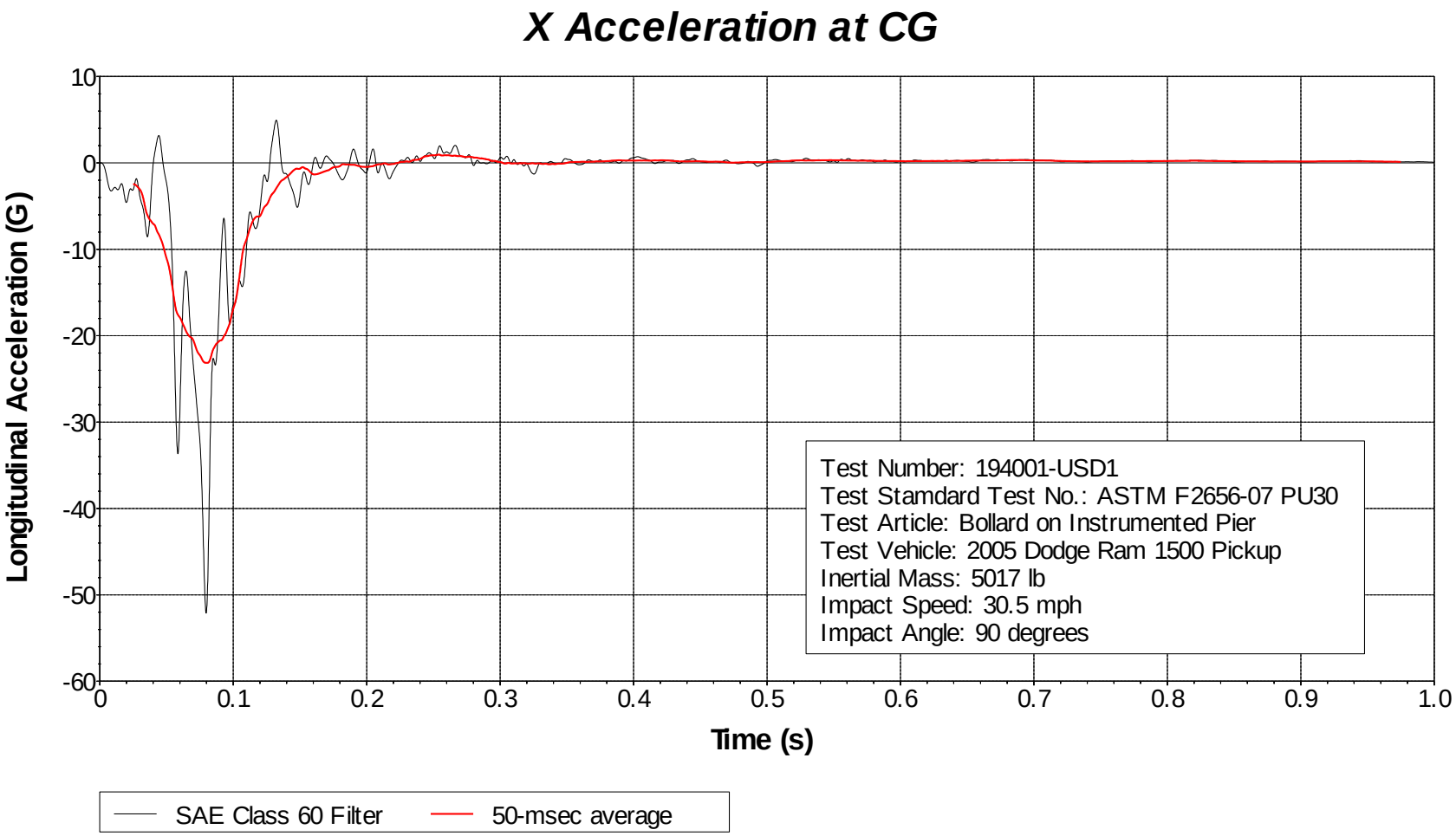

Figure A.5: Longitudinal Accelerometer Trace Measured at the Center of Gravity of the Test Vehicle (Brackin, Menges 2014).

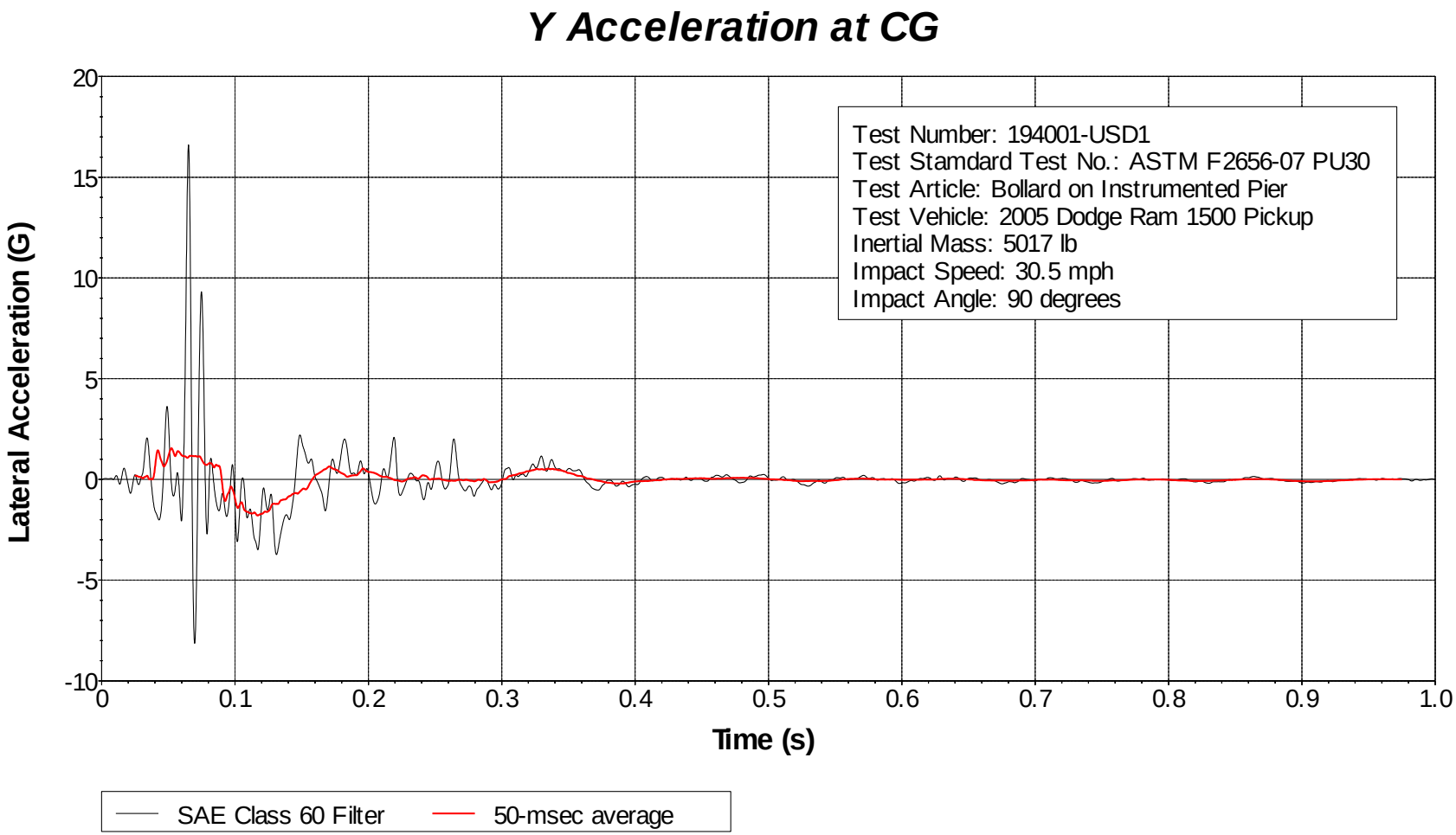

Figure A.6: Lateral Accelerometer Trace Measured at the Center of Gravity of the Test Vehicle (Brackin, Menges 2014).

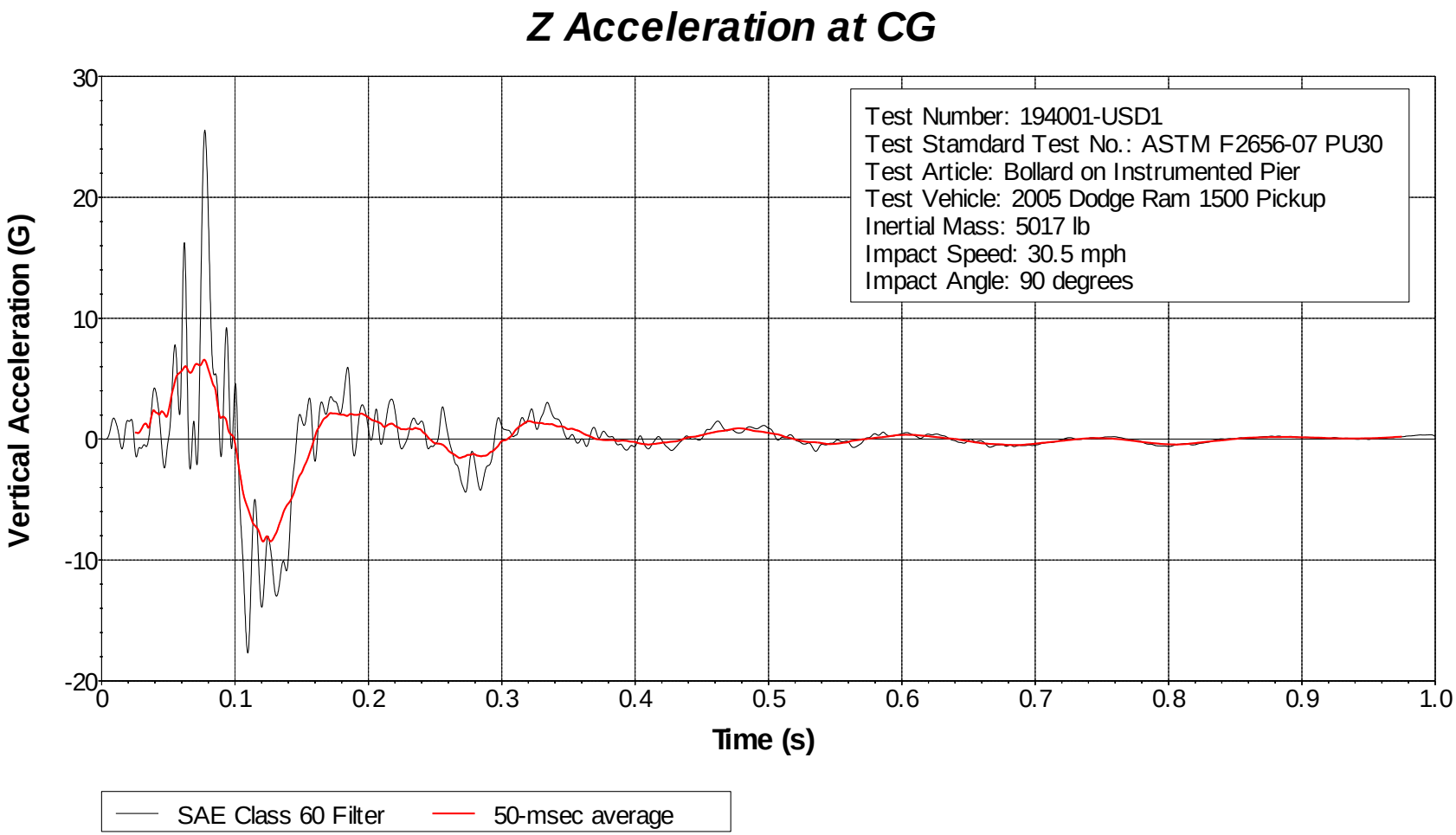

Figure A.7: Vertical Accelerometer Trace Measured at the Center of Gravity of the Test Vehicle (Brackin, Menges 2014).

APPENDIX B

SURROGATE VEHICLE DESIGN DRAWINGS

Conceptual design drawings for the surrogate vehicle and the structural frame are included in this section. Figure B.1 provides a general view of the idealized surrogate vehicle. It can be seen that the linear compression springs and the honeycomb assembly are attached securely enough to resist the applied load experienced during a full-scale crash test. Figure B.2 provides the overall dimensions of the structural frame. Figure B.3, Figure B.4, and Figure B.5 show detailed member lengths and general notes necessary for completion.

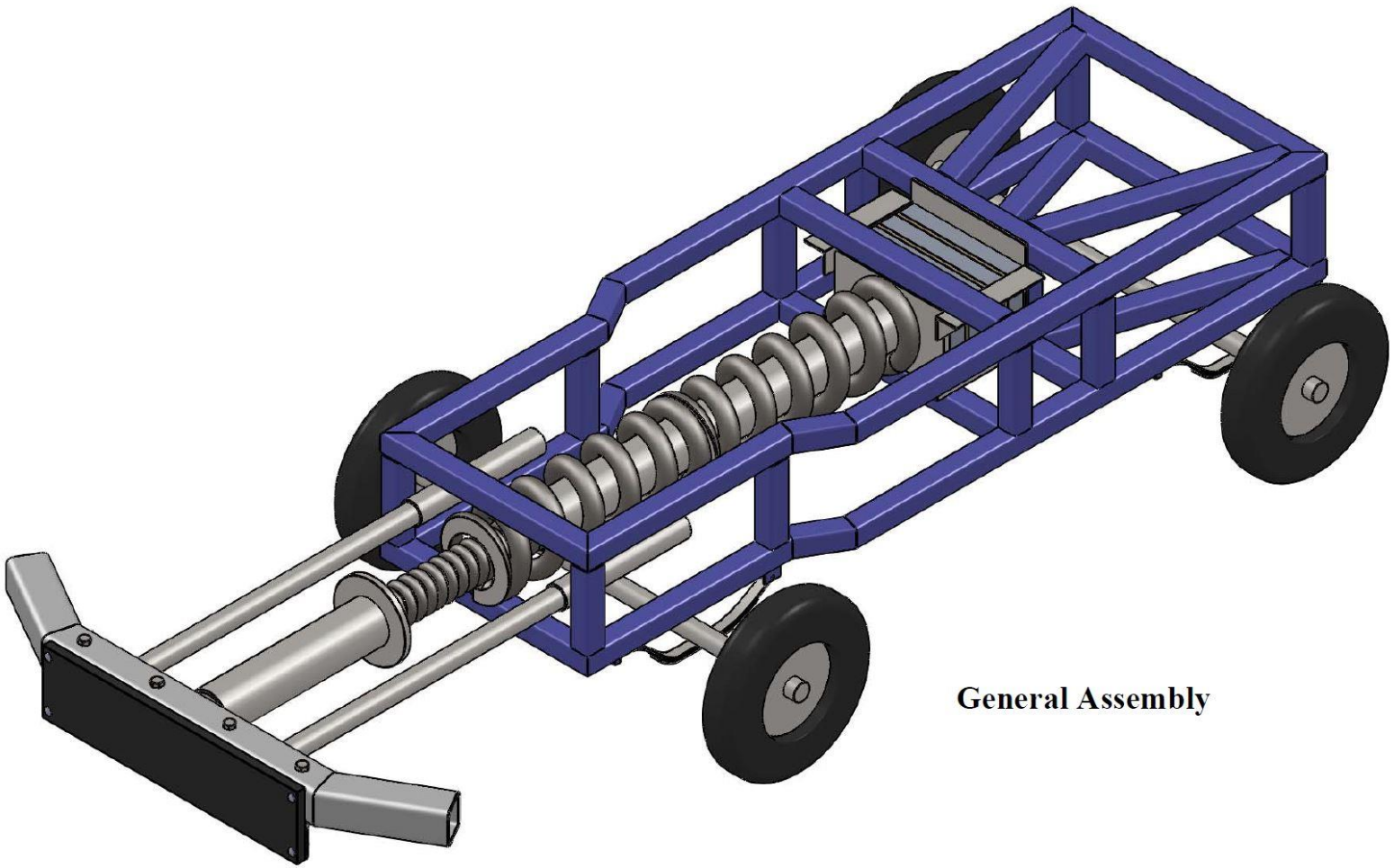

Figure B.1: Overall View of Low Speed Surrogate Vehicle Concept.

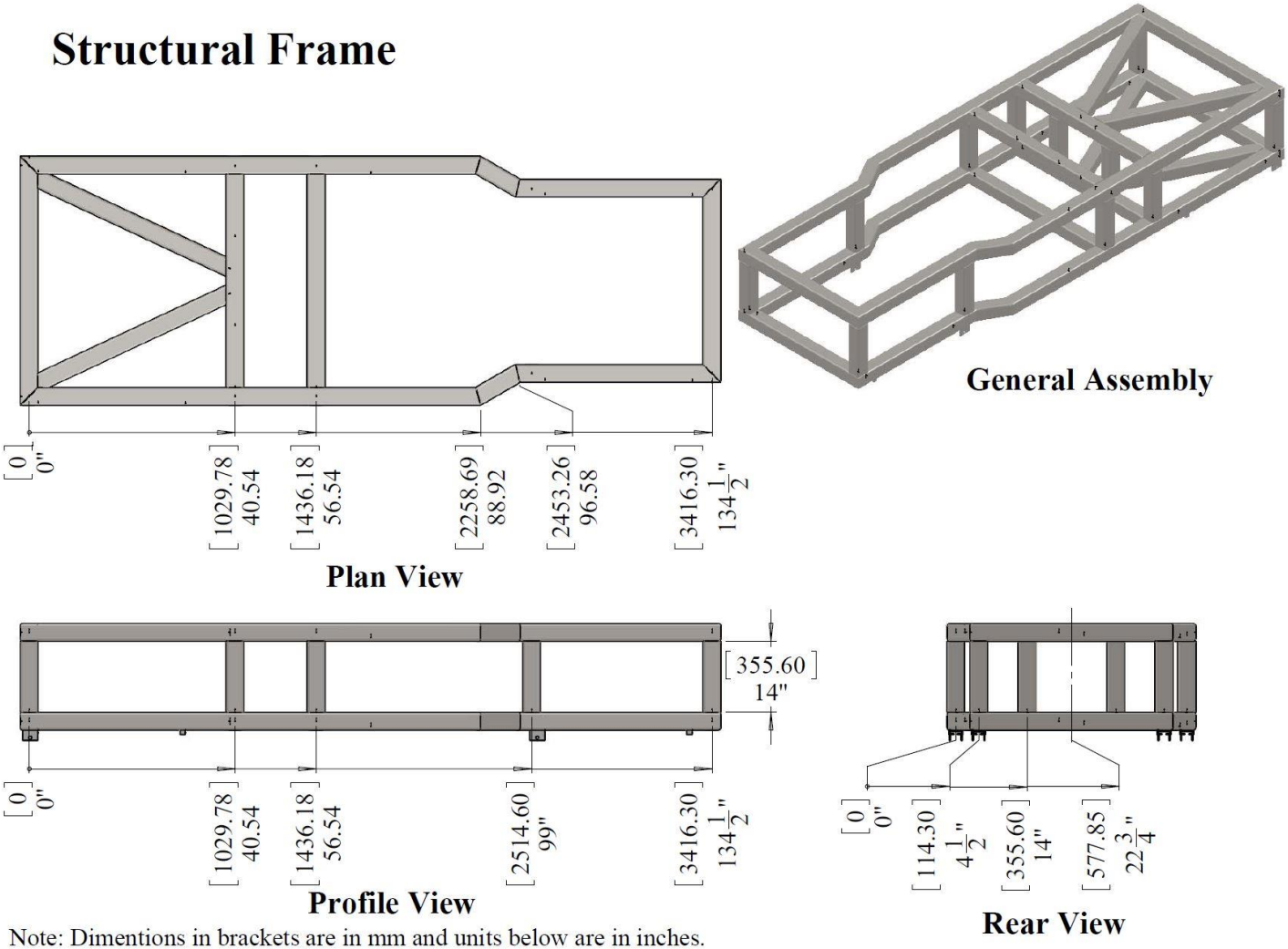

Figure B.2: General Dimensions of Structural Frame.

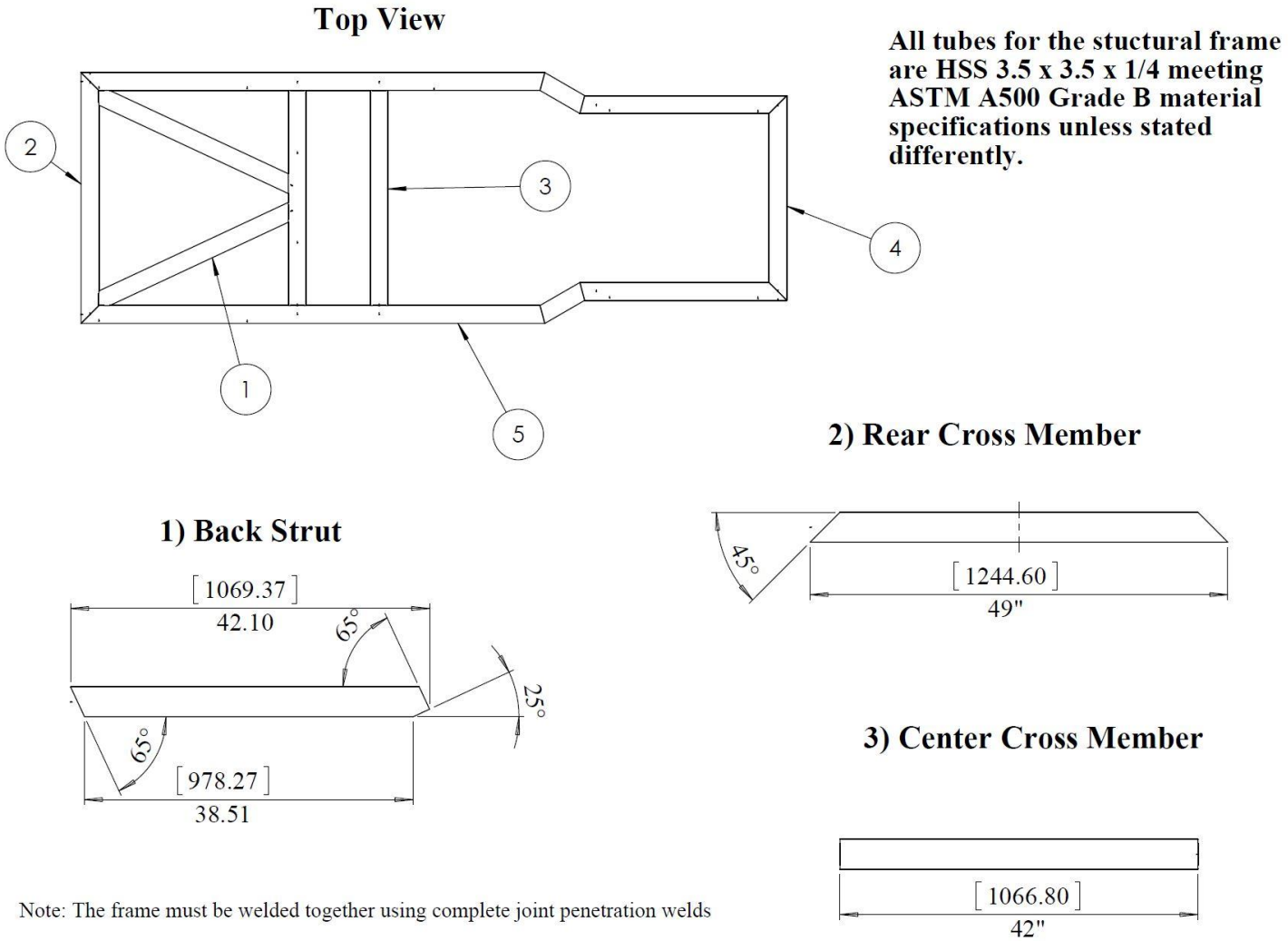

Figure B.3: Detail of Structural Frame Members.

4) Front Cross Member

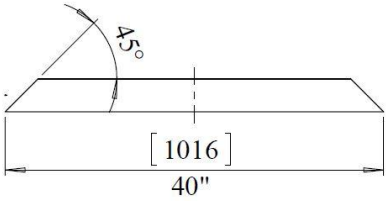

5) Side Member

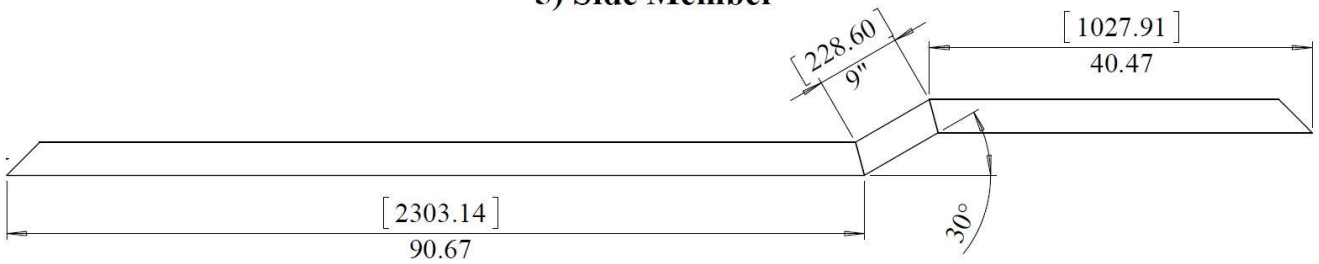

Note: The frame must be welded together using complete joint penetration welds

Figure B.4: Detail of Structural Frame Members.

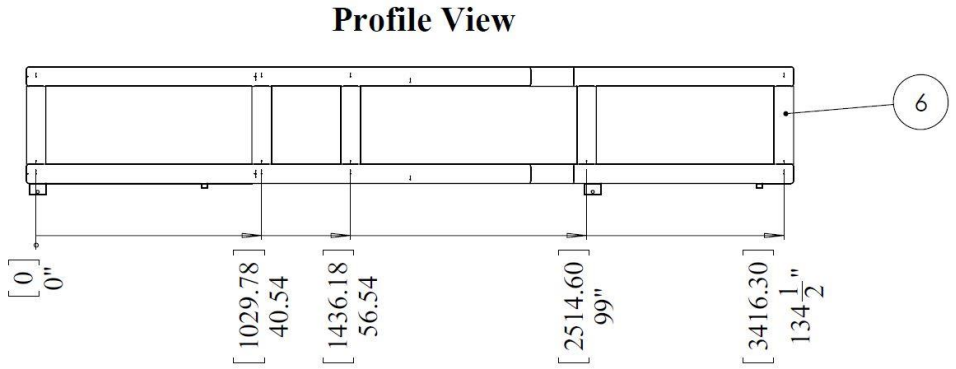

Note: The frame must be welded together using complete joint penetration welds

Figure B.5: Detailed Profile View and Vertical Member Detail.